UCLouvain

epl

École polytechnique de Louvain

Topology optimization of the electric motors for a Formula Student Race Car

Formula Electric Belgium

Author: **Thomas Clayson**
Supervisor: **Bruno Dehez**
Readers: **Aude Simar, Louis Beauloye**
Academic year 2022–2023
Master [120] in Electro-mechanical Engineering

Abstract

This thesis presents the results of a comprehensive study on the topology optimization of the electric motors dedicated to a Formula Student race. The motivation for this research arises from the need of Formula Electric Belgium, the former Formula Student team of the KUL University, to design their own motor concept, as opposed to using a motor from an industrial partner. The purpose of this research is to optimize the current design of the electric motors for maximum performance, efficiency, and weight reduction, with the goal of enhancing the overall power-to-weight ratio of the race car.

Using a combination of numerical simulations and optimization techniques, a systematic approach was developed to optimize the topology of the electric motors. Finite element method was employed to model the electromagnetic and structural behavior of the motors. Topology optimization was then applied to search for the optimal distribution of materials within the motor's rotor, aiming to minimize weight while meeting high performance and structural constraints. After that, a parametric optimization was used further down in the process to generate an optimal design of the new motors starting from the raw optimal topology.

The findings of this research contribute to the field of electric motor design and its application in the context of Formula Student racing. The optimized motor design can potentially lead to improved racing performance and enhanced competitiveness in the Formula Student competition. The methodology and findings of this study can provide valuable insights for future research and development for *Formula Electric Belgium"*s goal of designing their own motor concept.

Acknowledgements

I would like to express my deepest gratitude to my supervisor Bruno Dehez who in the first place allowed me to undertake this project and for providing valuable guidance, comments and suggestion throughout the course of the thesis.

I would also like to extend my sincere thanks to Louis Beauloye who guided my thought the optimization process and providing me with sufficient theoretical background to be able to work autonomously on the matter.

I cannot end this acknowledgement without mentioning the *Formula Electric Belgium* team. Thank you for this experience and for letting me be a part of that amazing and ambitious project. ’

Contents

List of Figures

List of Tables

List of Abbreviations

AM Analytical method 22

EMF Electromotive force 37

EV Electric vehicles 6, 15, 16, 18, 21, 27

FEB Formula Electric Belgium 10, III, V

FEM Finite element method 22, 24, 37

IPM Interior buried permanent magnets 8–10, 13, 15, 16, 20, 21, 35, 64, III, V

LCM Lower common multiple 15, 37

MMA Method of moving asymptotes 18, 20, 32, 70

MMF Magnetomotive force 9, 15

PM Permanent magnets 6, 36, 42

PMSM Permanent magnets synchronous motor 6–8, 22, 25, 38, IV, V

SIMP Solid Anisotropic Materials with Penality 18, 20, 31–34, 47

SPM Surface mounted permanent magnets 8

TO Topology optimization 17–19

1 | Formula Student

1.1 FSAE International

"Formula Student is a testing ground for the next generation of world-class engineers and one of the biggest student event around the globe. It is one of the most prestigious engineering competition for young students and it is organized by the Society of Automotive Engineers (SAE) International. This event is often viewed by the motorsport industry as the standard for engineering graduates, transitioning them from university to the industry" [1]

Figure 1.1: Formula Student Teams 2020 edition

Formula Student international competition

Formula SAE ® is an international competition organised each year by the SAE. The competition started first in the US and was introduced in Europe by 1998 due to the growing demand of young engineers with practical experience in terms of teamwork, design, manufacturing and project management. The international

competition takes place on diverse tracks all across Europe, where each team has to compete on a series of daily events. The main objective of this project is to inspire and develop enterprising and innovative young engineering students in Automotive. Each year, Universities and teams worldwide are challenged to design and build a single-seater, open cockpit and open wheel formula style race car. There are four main categories competing in Formula Student: Internal combustion cars, electric cars and hybrid vehicles.

Competition events

The competition is composed of a series of static and dynamic events that have been specifically designed to evaluate the performance of the vehicles, going beyond the conventional race format. The following description provides a brief overview of the different tasks the teams have to perform.

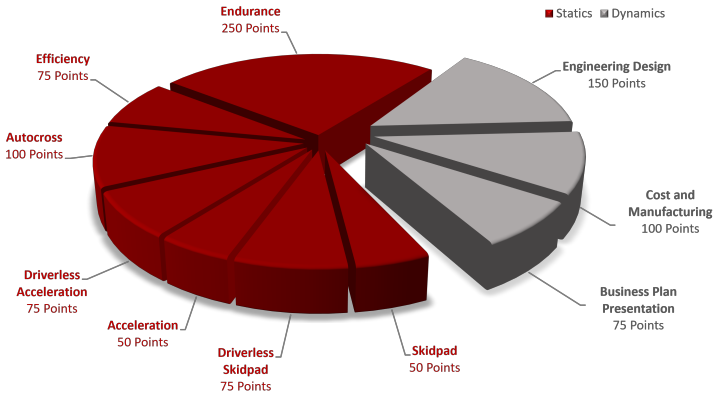

Figure 1.2: Points distribution between the different events

Static events

- Business plan: pitch meeting with potential investors where the team has 10 min to convince to invest in their business project with the idea to build 1000 units of their car each year.

- Cost: control of the documentation of the race car regarding manufacturing and assembly costs.

- Engineering design: 40 minutes presentation going through the car design, innovations and development to a panel of world class engineering judges. This event is one of the most prestigious and directly describes the team superior knowledge of engineering concepts.

Dynamic events

- Acceleration: 75 meters drag race designed to show the cars acceleration performance.

- Skid pad: the car has to drive on a full right hand circle followed by a full left hand circle. This event is designed to test the cornering performance of the cars.

- Autocross: one round lapped time on a circuit. This event is designed to test the ability of the drivers and also the track pace of the vehicles.

- Endurance: 22 kilometers race over 20 laps with one pit stop and a driver change after 11 kilometers. This event tests the overall reliability and performance of the vehicles.

- Efficiency: the race car efficiency is scored based on the energy consumption during the endurance event.

1.2 Formula Electric Belgium

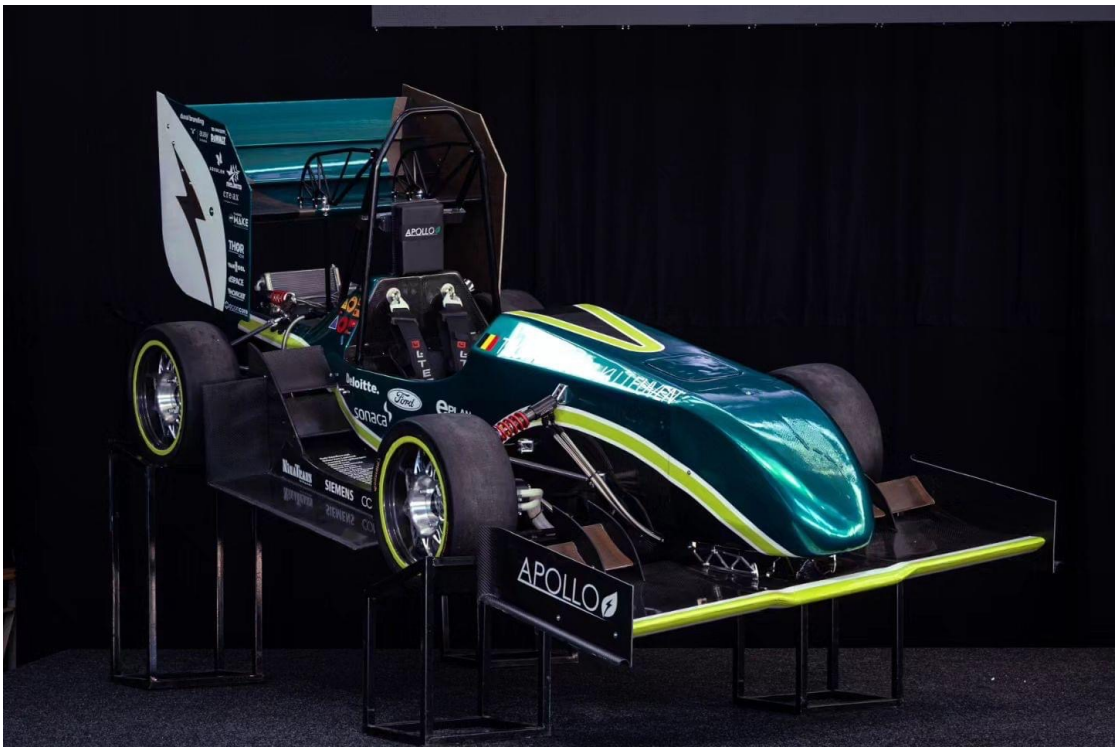

Figure 1.3: *Formula Electric Belgium* 2023 electric race car AURORA

Formula Electric Belgium is the former formula student team of the KUL University and Thomas More University. Based in Leuven, it is composed of 52 students from different educational backgrounds. The team is composed of full-time members, part-timers and thesis students. In addition, the team benefits from various partnerships, allowing them to access high-quality components and cutting-edge manufacturing processes.

The team is organised around six departments: Management, Electronics, Vehicle Dynamics, Powertrain, Composites & Aerodynamics, Research & Development, and finally Driverless. All the departments are intimately linked during the overall development of the race car. The thesis students compose the Research & Development department and are responsible of future innovations for the project.

Recently, *Formula Electric Belgium* expanded their research developing an autonomous race car. The objective is to participate in the recent Formula Student Driverless category. This project is still at its early stage but it is becoming increasingly important for the team, trying to explore the new possibilities of autonomous driving.

The work presented in this paper has been executed in the context of a master thesis in collaboration with the *Formula Electric Belgium* 2022-2023 team.

2 | Introduction

This chapter presents an introduction to the field of application of the thesis. We first detail the design of the powertrain and follow with a comprehensive overview of the electric motor technologies commonly found on the market. After that the current motor concept of the team is analysed. Finally coming from the development of the drive system, the thesis objective is presented and the research and optimization methodology is formulated.

2.1 Background

2.1.1 In-Wheel hub motor design

The formula style race car is powered by four independent electric motors. The drive system uses an in-wheel hub design, where the motors are directly mounted on the wheels that they are powering. This type of system is very common in electric vehicles for several reasons. One of the main advantages of using in-wheel hub motors in a race car is that they can provide independent control of each wheel, allowing for precise torque vectoring and traction control systems. This enhance the vehicle's performance in terms of acceleration, handling, and stability during cornering. All these aspects makes the car more competitive in the context of the *FSAE* competitions. In addition, the in-wheel hub design eliminates the need for a traditional drivetrain, which includes components like a transmission, driveshaft, and differential. This result in a simpler, lighter and more compact powertrain configuration.

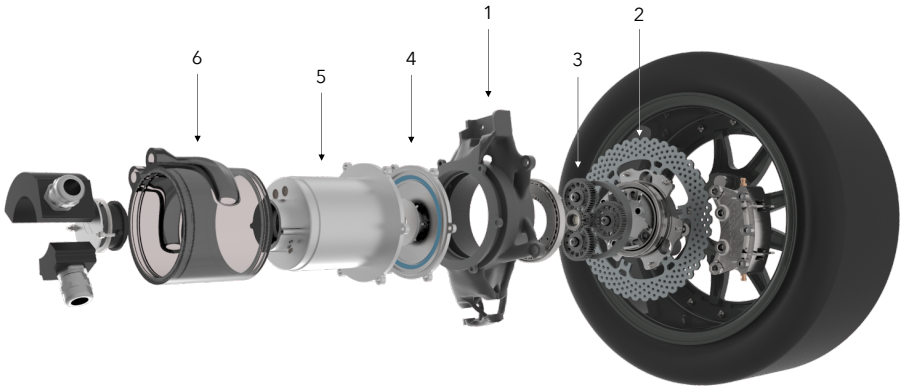

Figure 2.1: In-wheel hub design detailed view

The in-wheel hub drive system of the car is composed of multiple components and is represented in Figure 2.1. The connection between the car and the in-wheel system is provided by the upright (1). This component is the interface between the suspension control arms, the steering rod and the wheel hub. The upright is attached to the vehicle's suspension, supporting the weight of the car and allowing vertical movements of the wheel, while also transmitting the driving and braking forces generated by the in-wheel hub motor. Between the upright and the brakes (2) we have a set of planetary gears (3). This system is used as a gearbox, to convert the rotating velocity of the motors into additional torque. These types of formula style race cars are not designed for top speed performance but for maximum acceleration.

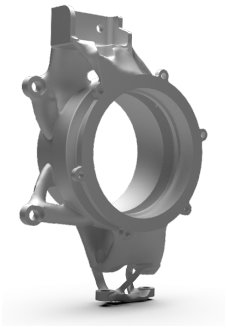

Figure 2.2: Upright

This explains why very high torque is desirable for such application. One of the main advantages of the planetary gearing system is that it is a high power density design, meaning it can handle higher torque and higher reductions in a smaller, more compact package. This system can also handle important shock loads and higher overhung loads because of the unique self-aligning properties specific to planetary gearing. Finally, the upright is connected to the motor plate (4), which serves as the fixation point for the housing case (5) of the electric motors. Each motor is covered by a cooling jacket (6) for thermal management aspects. The cooling jackets were previously studied and designed in collaboration with Diabatix, using generative design to create the most efficient channeling system inside the jacket to allow high heat transfer capacity.

Figure 2.3: Planetary gearing

2.1.2 Types of PM synchronous machines

Permanent magnets synchronous motor (PMSM) are widely used in the automotive industry for traction motors. These kinds of motors are known for their high torque density and high efficiency, making them appropriate for Electric vehicles (EV) applications. This section is intended to provide a overview of the types of PMSM technology used today. It is important to note that we will only consider radial machines (where the magnetic flux rotate along the radial direction of the motor) but axial flux motors are also a type of Permanent magnets (PM) machine that can be found in EV applications.

Exterior rotor PMSM and interior rotor PMSM

PMSM can be divided into two categories according to the relative position of the rotor and stator, namely a inner rotor PMSM and a external rotor PMSM. Figure 2.7 and 2.6 present the two configurations[1]. Inner rotor topologies are widely used in many applications since the static part is placed externally. The two configurations have both their own qualities and disadvantages:

Inner rotor PMSM

The inner rotor design offers advantages such as high power density, lower cogging torque, reduced weight, and efficient space utilization. Its compact size and smaller air gap contribute to a stronger magnetic field, higher torque density, and smoother operation. These characteristics make the inner rotor design well-suited for applications where size, weight, and torque performance are crucial factors.

Outer rotor PMSM

The outer rotor offers advantages such as a high torque-to-inertia ratio, improved efficiency due to reduced magnetic flux leakage and eddy current losses, and ease of integration with the vehicle's drivetrain. However, this configuration may require more space and add weight to the vehicle. The larger rotor diameter allows for higher acceleration and deceleration rates, making it suitable for applications that require quick changes in speed. Additionally, the outer rotor PMSM is typically installed outside of the transmission or drivetrain, directly coupled to the vehicle's wheels, facilitating integration into the overall system.

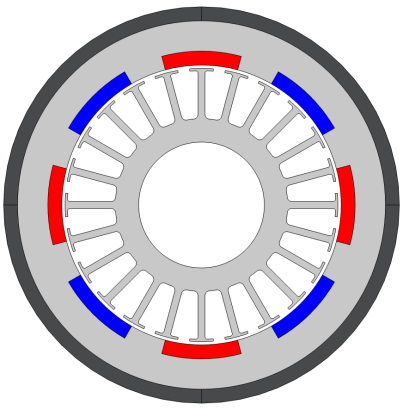

Figure 2.4: Outer rotor PMSM

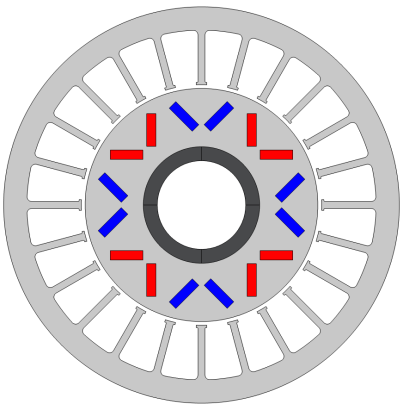

Figure 2.5: Inner rotor PMSM

[1]Throughout this thesis, the visual representation of the permanent magnets will employ a color scheme consisting of red and blue. The choice of distinct colors serves to differentiate between the two polarities of the rotor poles.

Interior buried PMSM and surface-mounted PMSM

We can distinguish two types of PMSM motors depending on the relative disposition of the permanent magnets: Interior buried permanent magnets (IPM) motors and Surface mounted permanent magnets (SPM) motors.

Interior buried PMSM

One of the key points of IPM design giving them an edge in vehicle applications like traction motors, is their high-speed performance. In these machines, the magnets are mechanically captured within the rotor lamination, making them suitable for high speed operation unlike SPM machines. In addition, these motors are defined by their relatively high magnetic saliency ratio ($L_q \neq L_d$). Due to the unequal reluctance between the d- and q- axis of the rotor, an IPM motor has the ability to generate torque by taking advantage of both the magnetic and reluctance torque components. This induce higher flux concentration, higher air gap flux density and in turn provides a torque increase in the machine. Finally these motors provide a much broader region of consistent torque.

Surface mounted PMSM

On the other hand, the surface mounted PM machine is of simpler structure, thus also widely used in many applications including electric vehicles. In a SPM machine, the magnets are mounted on the exterior of the rotor surface, meaning a strong adhesive is require to retain the magnets on the rotor. The weakened mechanical strength limits the motor's maximum safe mechanical speed, making them less suitable for high speed applications. In addition, these motors have very limited saliency ratio ($L_q \approx L_d$). Because of this near unity saliency ratio, SPM motors rely mainly, if not completely, on the magnetic torque component.

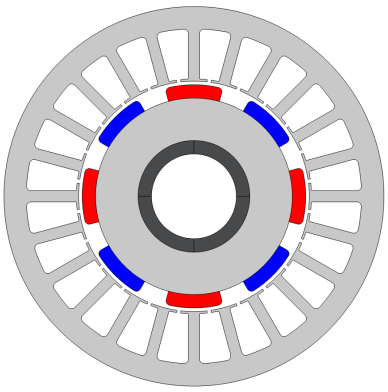

Figure 2.6: Outer rotor PMSM

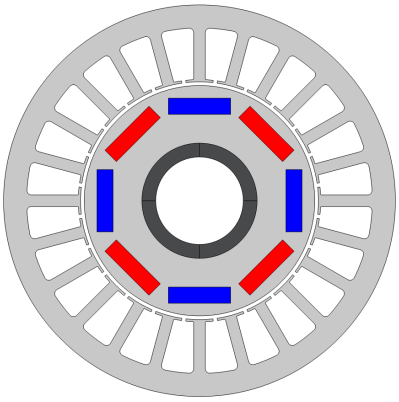

Figure 2.7: Inner rotor PMSM

However, unlike SPM motors, designing an IPM motor has been proven challenging due to the rotor structural complexity. The performance of such motors is

mostly influenced by the rotor shape, therefore, determining an appropriate IPM rotor topology is essential for designing a high power density, high speed motor.

Distributed winding and concentrated winding

There are two main types of stator windings commonly used in electric motors: distributed windings and concentrated windings.

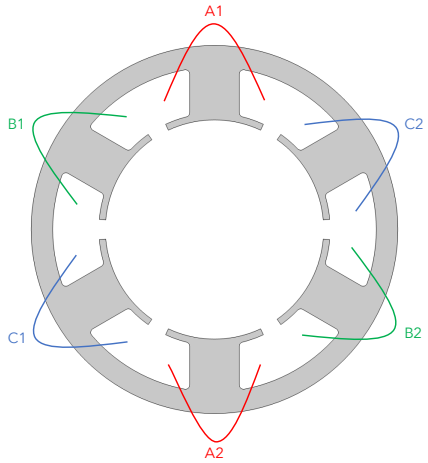

Figure 2.8: Concentrated windings

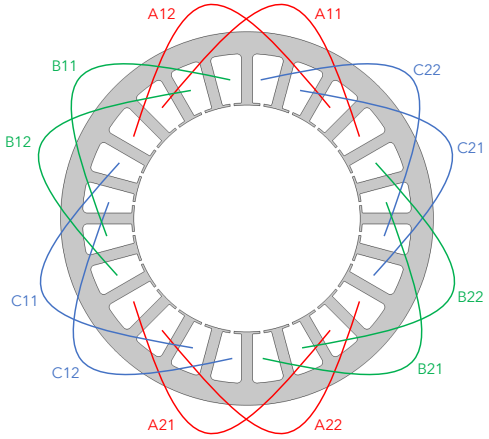

Figure 2.9: Distributed windings

Distributed windings

In a distributed configuration, the windings are divided into several coils that are distributed uniformly around the stator's circumference. This configuration is also know as overlapping with slots per pole per phase greater or equal to one. This means that each phase windings is distributed in several slots. The coils are either connected in series or parallel to form a closed loop.

Concentrated windings

On the other hand, a concentrated configuration consists of a single layer of coils that are placed around the stator's circumference. This configuration is also know as non-overlapping with slots per pole per phase smaller to one. This means that each phase windings is wound only over a single stator tooth. Like in a distributed winding stator, the coils can either be connected in series or parallel to form a closed loop. Figure 2.8 and 2.9 show a basic layout of the two windings configurations.

In general, distributed windings in PM machine have a lower harmonic content in the windings Magnetomotive force (MMF) reducing the pulsating component of the cogging torque. This makes them a very attractive design choice. Distributed windings machines also have higher power densities due to lower copper weights and

higher efficiencies obtain through lower copper losses for the same output power rating.

2.1.3 Electric motors concept of FEB

The current motors used by *Formula Electric Belgium* are provided by Fischer Elektromotoren. This company provides the complete stator and rotor package to the team.

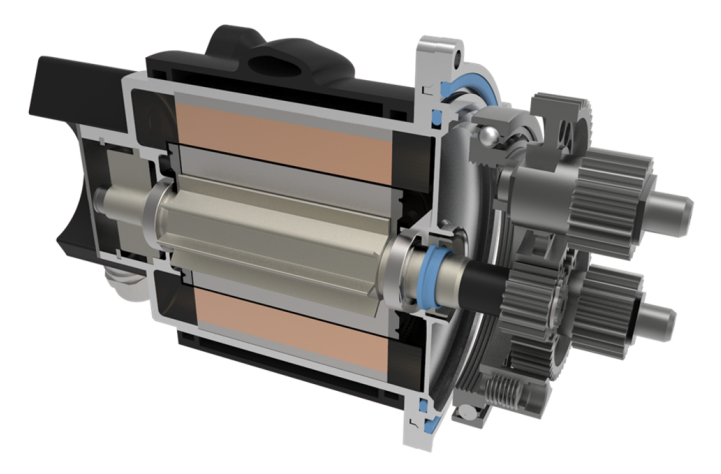

Figure 2.10: Cross section of the motor concept assembly

Figure 2.10 represent the complete mechanical assembly of the motors. The stator from the manufacturer is directly mounted in its casing and a resin is applied by potting to the end windings for electro-magnetic isolation and covering. The stator casing has multiple functions. Firstly, it is the surface directly in contact with the cooling jacket. Secondly, it is the attachment point for the motor cover plate and it incorporates a resolver for the controller unit.

The motor is a IPM type. The rotor is composed of eight Neodymium permanent magnet (NdFeB) placed in a spoke topology. Figure 2.11 presents an axial view of the rotor. The team is responsible of placing the rotor on the main shaft. Two balancing disks are then placed on each extremes of the rotor for proper balancing. Uneven weight distribution of the rotating components can cause the part's rotational center to be out of alignment with the geometric axis, inducing vibrations that can decrease the system's performance. The hole assembly is mounted on the upright, through the cover plate to form the complete drive sytem as presented previously.

Figure 2.11: Spoke rotor of FEB

The amount of information regarding the motor concept is very limited due to confidentiality agreements with the industry. This design is used by many other teams of Formula Student. Thus only the basic geometric quantities are known for the rotor and stator. The known parameters are summarized in table 2.1. On the other hand, the stator design (type of windings, number of slots, number of turns per slots) remain unknown. This will highly affect the design procedure and the comparison between the reference and optimized model. In section 3.1 we will develop the solution adopted to have the most accurate comparison between the current motor concept, and the optimized one.

Parameters	**Values**	**Units**
Number of rotor poles	8	Poles
Rotor Outer diameter	50.2	mm
Rotor Inner diameter	17	mm
Reference rotor mass	1	kg
Magnets dimensions	13.6 x 6 x 35	mm^3
Stator outer diameter	85	mm
Stator inner diameter	51.6	mm
Air gap length	0.7	mm
Reference mass	1.8	kg
Axial length of the motor	70	mm

Table 2.1: Motor parameters

2.2 Objective of the project

This thesis is motivated by the desire of *Formula Electric Belgium* to develop their own electric motors. In the competition context, the vehicle weight is one of the most important criterion in term of design choices. Each kilogram that can be saved can drastically improve the performance of the vehicle as a hole. In addition, these kind of formula style vehicle are designed for high acceleration, good cornering speed and handling. In a powertain, high acceleration is provided by high torque transmitted to the wheel. These aspects are very important regarding the different events at the competition meaning each component of the vehicle should be optimized to have the highest power-to-weight ratio possible. Keeping this in mind, the logical next step for the powertrain department was to explore the possibilities to develop the motors in house.

The main objective of this thesis focuses on the development of a new interior permanent magnet rotor, that improves the power-to-weight or torque-to-weight ratio of the current motors. The thesis will investigate the use of topology optimization tools to generate an optimal design of the rotor.

2.3 Research approach and methodology

The rotor optimization approach involves a systematic and comprehensive methodology aimed at improving the performance of the motor. The first step is to design a reference model that simulates the actual motor's performance. However, due to limited information about the real reference spoke motor concept, a careful approach is taken to ensure that the reference model is as representative as possible.

Once the reference model is established, the next phase involves numerical modelling and topology optimization. This step utilizes advanced computational techniques to generate multiple sets of topologies. Each set consists of various designs, where the overall rotor mass is kept constant as a constraint. Through this optimization process, the composition of permanent magnets and iron in the rotor is systematically varied to identify the most optimal structure.

Following the topology optimization, the focus shifts towards refining the optimal topology design. This refinement stage takes into account the specific powertrain configuration, particularly the in-wheel design of the race car. A tailored solution is developed to seamlessly integrate the optimized rotor design with the existing powertrain, ensuring compatibility and efficiency.

Once the refined design is established, an in-depth analysis is conducted to evaluate its performance. This analysis involves assessing various factors such as torque-to-weight ratio, cogging torque, and harmonic content. Limitations encountered during the optimization process are carefully examined and discussed, providing insights into potential areas for further improvement.

3 | State of the art

This chapter provides a comprehensive overview of the existing knowledge and research related to topology optimization and rotor design of electric motors. It reviews relevant literature and research papers to establish the context and significance of the research study.

3.1 Reference topology

As explained in subsection 2.1.3, very limited amount of information is known about the current electric motor concept used by the team. To perform a pertinent development of a new rotor topology, we need a reference model with which we can compare our results and see if the performance was enhanced.

As previously mentioned, the existing motor in use is an IPM motor, featuring a rotor with a spoke topology consisting of eight poles. Through a comprehensive analysis conducted by MagCam, we have obtained information regarding the quantity of magnets employed for each magnetic pole in the motor. However, the main limitation lies in the lack of information regarding the stator configuration. Without knowledge of the stator design, it is not feasible to optimize our new motor using the same stator geometry currently employed. Although the research project primarily focuses on developing a new rotor design, the optimization process becomes less meaningful when comparing two distinct rotors that are individually optimized for their respective stators. In order to address this issue, we have devised a standard stator configuration, referred to as the reference statoric geometry. In subsection 3.1.1, we provide a detailed explanation of the design choices made for the reference stator element, which will serve as the benchmark throughout the entire project.

To finalize the construction of the reference motor, the inclusion of the rotor element is required. For this purpose, we used the already known parameters and coupled them with a spoke topology rotor consisting of eight magnetic poles, with a predetermined magnet quantity and optimized specifically for the new stator configuration. By doing so, we aim to achieve an optimal combination of the spoke rotor and stator assembly, which accurately reflects the current motor concept used by the team. This assembly will serve as our reference model throughout the study.

Figure 3.1 and 3.2 depicts the resulting rotor and stator assembly. As mentioned

above, the spoke rotor design was carefully optimized to maximize its performance when paired with the reference stator. In subsection 5.2.3, we will elaborate on the optimization strategy employed in order to facilitate a meaningful comparison with the results obtained from the topology optimization.

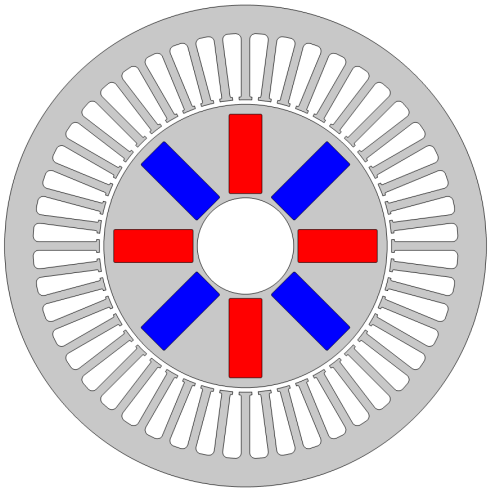

Figure 3.1: Reference rotor and stator model

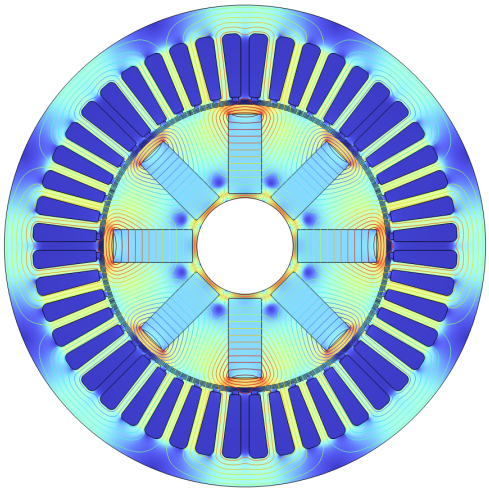

Figure 3.2: Magnetic flux and magnetic potential A_z solution

3.1.1 Stator model for analyzing rotor properties

The reference stator is composed of 48 slots and single layer distributed windings. For such design, the number of slots per pole per phase q is equal to two. Figure 3.3 illustrate the stator design.

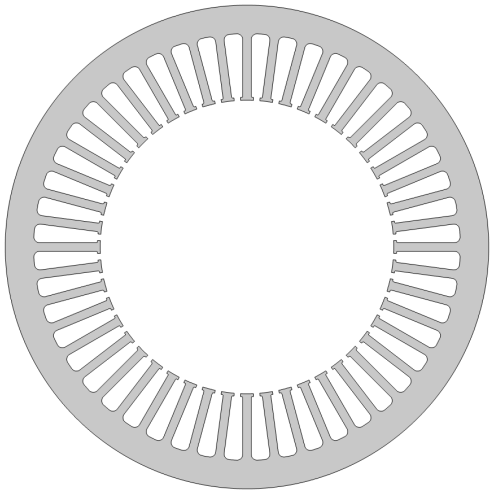

Figure 3.3: Reference stator part

The design choices for the reference statoric element are justified as follows:

- As discussed in subsection 2.1.2, the decision to adopt distributed windings for the reference stator is supported. This configuration offers several advantages, primarily the reduction of MMF harmonics content. By utilizing distributed windings, the stator can closely approximate a sinusoidal magnetic field waveform in the air gap. This leads to smoother operation and a decrease in the presence of MMF harmonics, thereby enhancing overall performance.

- An important design consideration for the reference stator is the determination of the number of slots and rotor poles. In this case, it is noteworthy that the Lower common multiple (LCM) between these two quantities is found to be 48. Opting for a design with a higher LCM value is advantageous as it promotes a reduction in the torque ripple content. In the context of the motor size under investigation, an LCM value of 48 can be considered substantial. For a comprehensive understanding of the significance of the LCM factor on the cogging performance, please refer to subsection 4.3.2 where detailed insights are provided.

- Lastly, it is important to consider the maximum achievable winding factor (k_w) for the design choices of the motor. k_w has been determined to be 0.966 for the chosen configuration. The winding factor represents the ratio of the flux linked by a specific winding to the flux that would have been linked by a single-layer full-pitch non-skewed distributed winding with the same number of turns and one slot per pole per phase [2]. Essentially, the winding factor quantifies the performance of the windings.

  In the context of electric motors, the torque generated is proportional to the fundamental winding factor. Therefore, a higher value of k_w is desirable as it indicates enhanced performance. Table 3.1 presents the maximum achievable fundamental winding factors for different combinations of stator slots (nSlots) and number of rotor poles (nPoles).

nSlots/nPoles	4	6	8	10
36	0.96	0.966	0.945	0.942
39	0.954	–	0.954	0.954
42	0.953	–	0.953	0.953
45	0.955	0.951	0.95	0.945
48	0.958	–	0.966	0.954
51	0.955	–	0.951	0.955

Table 3.1: Maximum possible fundamental winding factor

3.2 Rotor geometry of IPM motors

When considered IPM motors, many different topologies have been proposed. In a particular study [3], a thorough comparison of rotor shapes for EV applications

was conducted with the aim of establishing a design standard for traction motors. The study analyzed and compared the performance of three motor models from prominent EV manufacturers currently in production, along with two hybrid models.

Figure 3.4 illustrates the different rotor structures that were compared in the study. The objective was to assess the performance characteristics and identify the most suitable rotor structure for EV traction motors.

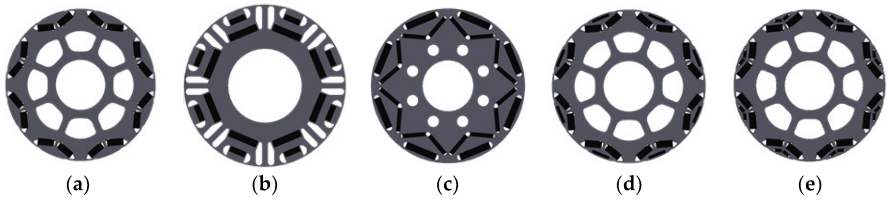

Figure 3.4: Five different shapes of IPM rotors: (a) V shape from manufacturer T; (b) double magnet shape from manufacturer V; (c) delta shape with a bar magnet in a V shape; and (d,e) improved shapes using a delta shape and a double V shape, respectively. [3]

In this comparative study, all of the motors being compared have identical dimensions, with the only variation being in their internal designs structure. To ensure optimal comparability of the results, simulations were conducted using the same stator design.

The findings of the analysis are summarized in Figure 3.5. However, it is important to approach these results with caution, considering that each rotor structure utilizes a different quantity of magnets, highly affecting their performances. Despite this limitation, certain conclusions can still be drawn.

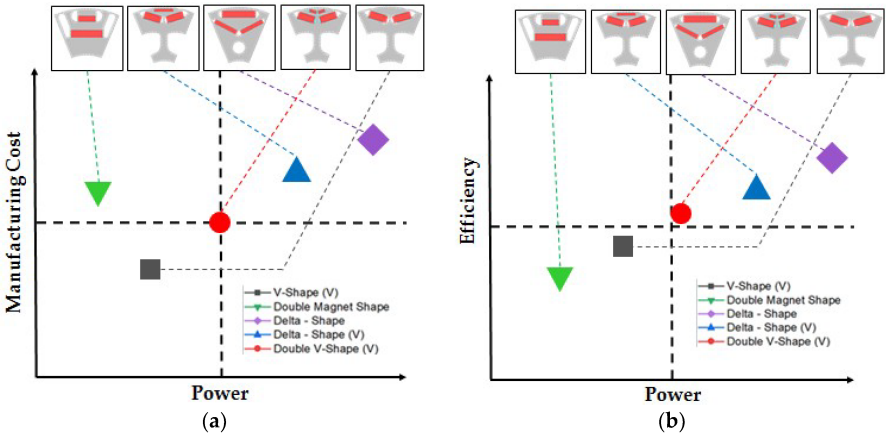

Figure 3.5: Comparison of power and other factors: (a) Comparison of manufacturing cost and power; (b) Comparison of efficiency and power. [3]

The study indicates that V-shaped rotors demonstrate outstanding performance while effectively minimizing the quantity of magnets employed. It is worth noting

that the manufacturing cost is of less concern for our study since the limitation of magnet usage is not as stringent as it would be for mass production scenarios. Nevertheless, we can infer that V-style rotors exhibit excellent torque performance and offer a lightweight design, aligning well with the objectives of the thesis.

Considering the utilization of topology optimization in our research, it is important to note that the selection of a specific rotor topology for optimization is not necessary. This is because the solver in topology optimization has the freedom to explore and determine the most optimal design without predefined constraints on the rotor topology. However, it is reasonable to anticipate that similar results may emerge from the optimization process, showcasing characteristics resembling the V-shaped rotor topology discussed earlier. Through topology optimization, we can expect to observe comparable outcomes in terms of performance, such as good torque performance and lightweight design.

3.3 Optimization techniques

There are several types of optimization methods commonly used in the industry. They can generally be categorized as follows:

- **Parametric optimization**: it involves optimizing a set of design parameters, such as material properties, geometric dimensions while keeping the overall design of the topology fixed.
- **Shape optimization**: it involves optimizing the shape of a design to achieve the best performance, while keeping other design parameters fixed.
- **Topology optimization**: this technique involves optimizing the distribution of the material within a given design space to achieve the best performance. The design space is typically discretized into small elements, and the optimization solver determines the optimal material density for each of these elements.
- **Generative optimization**: this technique involves using algorithms to generate and explore many potential design solutions that meet a set of performance criteria and requirements. [4]

Taking these considerations into account, Topology optimization (TO) offers several advantages compared to more traditional optimization techniques:

1. Efficient material utilization: it allows for the optimal distribution of materials within a given design space, resulting in more efficient and lightweight designs.
2. Exploring a large design space: TO has the ability to explore a wide range of design possibilities, often generating unconventional and innovative solutions. It is not limited by pre-defined design parameters, allowing for the discovery of novel and non-intuitive designs that may not have been considered through traditional optimization approaches.

3. Early stage design efficiency: this technique is particularly effective in the early stages of the design process, when many design variables and unknowns persist. It helps in exploring different design options and identifying promising solutions without being constrained by preconceived notions or assumptions.

3.4 Topology optimization for electric motors

Topology optimization has already been widely proven for electric motors applications. This type of optimization has been used in many studies providing pertinent results especially for EV applications, where usually a light weight and efficient design is required.

Density-based method is the most common formulation used to solve topology optimization problems. The density-based approach is derived from the homogenization approach [1] which is an essential branch in topology optimization methods. A particular density-based method widely used in structural and magnetic problems is the Solid Anisotropic Materials with Penality (SIMP) . A notable approach involves the combination of the SIMP method and the Method of moving asymptotes (MMA) solver.

The SIMP method allows for the representation of multiple materials within the design space, enabling the identification of optimal material distribution based on predefined objectives and constraints. By assigning penalization factors to different materials, the SIMP method effectively promotes the selection of the most favorable material distribution.

The MMA solver, on the other hand, is a popular optimization algorithm employed in topology optimization problems. It utilizes the concept of moving asymptotes[2] to iteratively update the design variables and converge towards the optimal solution. The MMA solver is particularly effective in handling multiple design constraints and facilitating efficient convergence in complex optimization problems.

More detailed information regarding the SIMP method and the MMA solver for optimization problems can be found in section 4.2.

In study [9], the torque performance of a synchronous reluctance motor is enhanced by using a SIMP-based method and the MMA algorithm. Figure 3.6 present an example of the resultant solution. In [11], a structurally stable rotor is

[1]The homogenization method is the earliest TO solution, first introduced in the 1980s [5][6]. In 1988, Bendsøe and Kikuchi proposed a homogenization approach based on the homogenization theory and numerical methods, which was a development for TO [7]. [8]

[2]Method based on a special type of convex approximation. In each step of the iterative process, a strictly convex approximating subproblem is generated and solved.The generation of these subproblems is controllcd by so called 'moving asymptotes',which may both stabilize and speed up the convergence of the general process. [10]

developed using density-based methods, and a functional prototype is manufactured.

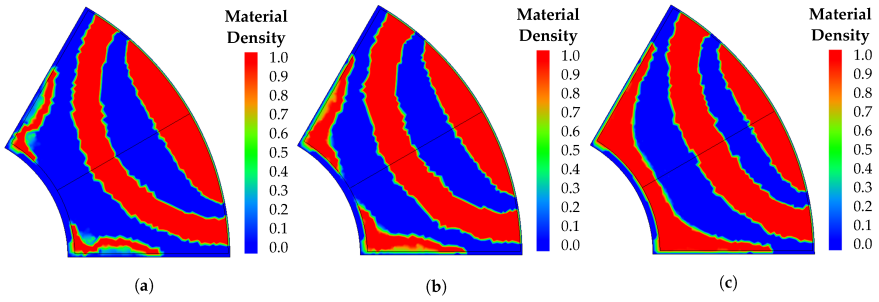

Figure 3.6: Different material density distributions using SIMP-based method with MMA solver. [9]

The ON/OFF method is another branch of TO, which uses discretized grids for electromagnetic devices. The ON/OFF method is a technique that uses a binary encoding. In this approach, each cell in the grid is represented with a binary number, while density-based methods commonly use continuous values of densities. Therefore, the ON/OFF method can take advantage of evolutionary algorithms[3] in the TO process. The ON/OFF method is also often used to convert a continuous density field into a binary material distribution for post-processing purpose.

In [12], the authors use an hybrid genetic algorithm[4] with the ON/OFF method to optimize the shape of a rotor's poles aiming to reduce the cogging torque. The solutions obtained from the ON/OFF method in [12] are illustrated in Figure 3.7. In [13], different rotor topologies are explored using genetic algorithms coupled with the ON/OFF method based on a normalized Gaussian network[5].

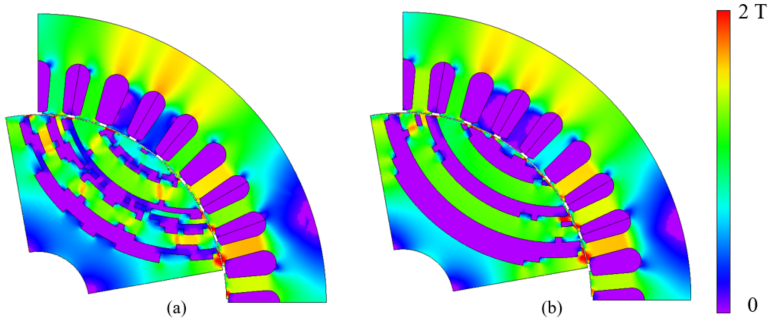

Figure 3.7: Shapes and magnetic flux density from an ON-OFF method. [12]

[3]Generic population-based metaheuristic optimization algorithm that uses mechanisms inspired by nature and solves problems through processes that emulate the behaviors of living organisms. [15]

[4]Metaheuristic inspired by the process of natural selection that belongs to the larger class of evolutionary algorithms. [16]

[5]The Normalized Gaussian Network (NGNet) model is a type of neural network used for classification tasks. It employs a Gaussian activation function and normalization techniques to capture complex patterns and nonlinear relationships in data. [14]

It is important to note that the previous paragraphs provided a general overview of commonly used methods and solvers in topology optimization, but not an exhaustive list. The intention was to provide a glimpse into the typical practices of the field.

For the purpose of this optimization research paper, we will employ the SIMP density-based method in combination with the MMA solver. This approach has been chosen due to its compatibility with the simulation software, *Comsol Multiphysics®*.

3.4.1 Uni-material topology optimization

In many research, uni-material topology optimization is exploited. This kind of study refers to a type of topology optimization problem in which the goal is to determine the optimal distribution of a single material within a given design space. In the context of rotor parts, uni-material topology optimization can be employed to find the optimal distribution of either iron or magnets while keeping the other component intact.

In [17], the torque performance of an IPM motor is optimized using uni-material topology optimization to find the best distribution of iron in the rotor yoke. Figure 3.8 illustrate the optimized models.

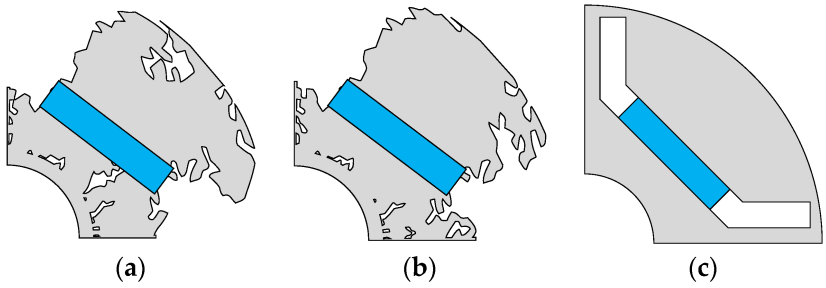

Figure 3.8: Rotor topologies and the reference model from study [17]. (a) first optimized model and (b) second optimized model, (c) is the reference

In [18] uni-material topology optimization is used to reinforce the structural integrity of a synchronous reluctance motor to be use in a high-speed application. The optimization is used to find the optimal placement of the additional iron needed to diminish the maximum stress point inside the rotor. Figure 3.9 present the research findings.

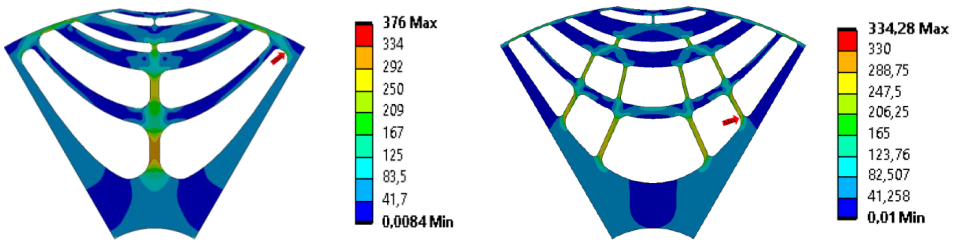

Figure 3.9: Reference and optimized rotor model: von-Mises stress [MPa]. [18]

3.4.2 Multi-material topology optimization

In contrast with an uni-material optimization, multi-material topology optimization refers to the type of topology optimization problem in which the goal is to determine the optimal distribution of two or more materials. The objective is to determined the optimal shape and distribution of the materials that will achieve the desired performance. Multi-material topology optimization is typically more complex than a uni-material topology optimization, as it involves determining the optimal distribution of multiple materials with different properties and interactions. The resulting designs may exhibit complex and heterogeneous material distributions. For a rotor design, this optimization approach allows us to explore novel and innovative rotor designs by enabling the solver to determine the optimal placement of magnets, iron, and air pockets.

In study [13], a multi-material optimization was used to maximize the average torque while minimizing the amount of permanent magnets required in a IPM motor. Figure 3.10 present different configurations obtained with this study.

Figure 3.10: Different resultant rotor shapes: the light red and darker red regions represent magnets with different remanent flux orientation. [13]

In the keynote [19], an electric motor for an EV application by Volkswagen Group Technology is completely designed using a multi-material topology optimization study.

In our pursuit of designing a new rotor structure through topology optimization, our approach will begin with a totally blank model. We will adopt a multi-material optimization approach, allowing the solver to optimize each element that constitutes the rotor design. This methodology allows to explore and optimize the distribution of materials within the rotor, enabling us to uncover an innovative and efficient rotor design.

4 | Numerical modelling of PM motors

The objective of this section is to present the theoretical foundations and practical implementations utilized in the design and analysis of the new motor. Each section will begin with a concise theoretical overview and then delve into the specific application of the topic in the numerical modeling of the motor.

4.1 Finite Element Methods

When conducting a detailed analysis and design of permanent magnets synchronous machines, multiple modeling approaches can be employed. Two commonly used methods are the Analytical method (AM) and the Finite element method (FEM). Finite element methods have gained significant popularity due to their ability to simulate complex geometries and scenarios that are challenging to solve analytically. The analytical methods have certain limitations in capturing specific effects. These limitations include:

- Geometrical complexity
- Non-linearity of materials behaviors and anisotropy
- Transient effect and coupled physics
- Optimization aspects

In addition, the mathematical complexity of analytical models and the inaccuracy due to simplified assumptions makes the FEM much more suitable. The scope of this thesis is limited to use of 2D finite element methods for optimizing and analysing a PMSM.

Basic theory

The theory of FEM is a numerical technique used to solve partial differential equations. The underlying principle of FEM involves dividing the system into small and simple elements, referred to as nodes, which can be individually modeled and solved. By solving the equations for each element and combining their solutions, an approximate solution for the entire system is obtained. While the detailed procedures for solving each finite element and assembling the global solution are

beyond the scope of this section, further information on these aspects can be found in [20].

4.1.1 Comsol Multi-Physics®

To perform the topology optimization and the performance analysis of the electric motors, we will use the software Comsol Multiphysics®. This software is a general-purpose simulation tool that enables the implementation of fully coupled multi-physics and single-physics modeling. Furthermore, the software's optimization module provides dedicated tools for parameter, shape, and topology optimization techniques.

4.1.2 FE model for PM machine

This subsection present the routine followed to model an electric motor in *Comsol Multiphysics®* and to setup the optimization study.

Geometric model

The initial step in the modeling process is to define the geometry on which the physics will be solved. In our case, we obtained the initial geometric quantities from the current motor concept used by the team.

The topology optimization is performed on a model that represents only one-eighth of the complete motor. This approach is adopted to significantly reduce computational time by taking advantage of the symmetries present in our motor design. Since our motor has eight rotor poles, each symmetry sector represents a 45[°] span.

Figures 4.1 present the geometrical model on which all the computations are carried out. It is evident to notice that the rotor sector is divided into multiple regions. The rationale explanation behind this division and its significance will be elaborated in subsection 5.1.2.

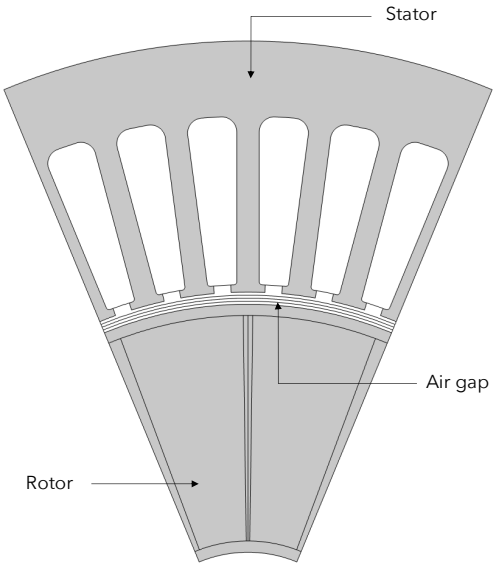

Figure 4.1: Geomtry of the optimzed model

In the design of the base model, a deliberate choice was made to align the rotor d-axis (magnetic axis) with phase A of the stator windings. This alignment serves the purpose of simplifying the representation

of the relative angle between the phasor of the three-phase system and the magnetic axis of the rotor. By aligning these axes, the electrical phase angle of the system can be easily determined. Figure 4.2 illustration the magnetic arrangement of the system.

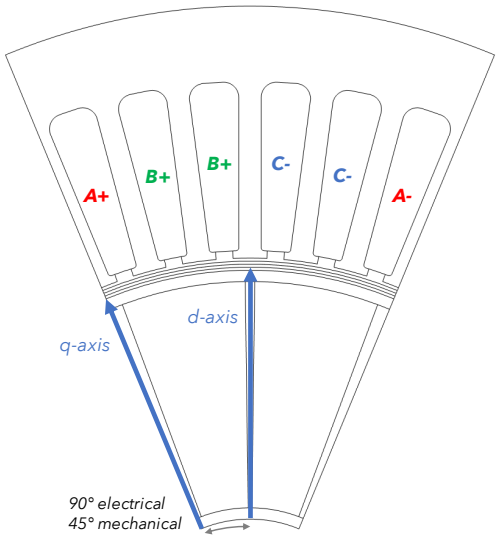

Figure 4.2: Magnetic configuration

The angle between the rotor d-axis and the phasor of the stator windings corresponds to the electrical phase angle of the system. In the optimization section, we will explore the use of the electrical phase angle as an optimization parameter. While the rotor d- and q-axes are fixed, the electrical phase angle becomes a degree of freedom that can be adjusted during the optimization process. By aligning the rotor d-axis with phase A of the stator windings in the base model, we establish a clear reference for the electrical phase angle. Subsection 4.3.1 delves into the specific reasons why this choice was made and further elaborates on its implications on the motor performances.

It is worth noting that in our modeling approach, the motor shaft and external casing are not included in the simulation. This decision is based on the assumption that their magnetic effects on the overall performance of the motor can be considered negligible.

Materials assignments

The subsequent stage in the numerical modeling involves assigning the appropriate materials to their corresponding geometric domains. To setup the topology optimization, we will consider three different materials: soft iron, air and permanent magnets. In subsection 4.1.3, we will provide a comprehensive overview of the electromagnetic and mechanical properties of all the material considered.

Generating the mesh

Finite element method (FEM) employs a discretization technique to approximate the geometry of the problem using finite elements. These elements can take the form of triangles, quadrilaterals, or other shapes depending on the model. The problem is solved on each of these elements and the global solutions is built from the combination of theses individual solutions. The result from the approximated geometry is called the mesh. The number of mesh points or mesh elements highly influences the accuracy of the numerical calculations. If the mesh is fine (high

number of elements) the accuracy of computation is high but the computational time will be high as well. Therefore a compromise has to be made between accuracy and time-consumption.

The following steps are necessary to ensure good balance between computational accuracy and time consumption for the FEM simulation of the permanent magnet synchronous motor.

1. Finer mesh in the air gap for an accurate torque computation
2. Refinement of the mesh near the edges of the rotor and stator to avoid numerical instabilities
3. Usage of coarser mesh nodes on other elements to reduces computational time

During the optimization process, triangular elements with a maximum size of 0.5 [mm] will be used within the rotor. This choice was made to ensure that the element size is approximately one hundredth of the maximum dimension of our system, providing a good balance between accuracy and computational efficiency for the topology optimization. For the stator part, an automated meshing will be employed, which will generate a suitable mesh based on the geometry. Finally, in order to accurately capture the complex magnetic field distribution across the air gap, the mesh density in this region will be refined. This is particularly important for torque computation purposes. The refinement involves dividing the air gap into multiple layers, allowing for a more precise representation of the magnetic field behavior.

Physics

To simulate the motor, two physics will be considered: electromagnetism and structural mechanics.

In the electromagnetism aspect of the simulation, the governing equations are based on Maxwell's equations and Ohm's Law. In the 2D model of the PMSM, these equations are solved by the software on each finite element. The computed variable in this physics is the magnetic potential vector, denoted as A. Table 4.1 provides an overview of the governing equations for electromagnetism in their differential form:

Maxwell's equations	
$\nabla \cdot D = \rho$	Gauss' law (electric)
$\nabla \times E = -\frac{\delta B}{\delta t}$	Faradays' law
$\nabla \cdot B = 0$	Gauss' law (magnetic)
$\nabla \times H = J + \frac{\delta D}{\delta t}$	Maxwell-Ampère's law
$\nabla \cdot J = -\frac{\delta \rho}{\delta t}$	Continuity equation
$\nabla \times A = B$	Magnetic vector potential

Table 4.1: Governing equations for electromagnetism

where H is the magnetic field strength [A/m], B is the magnetic flux [T], J is the current density [A/m^2], σ is the material conductivity, E is the electric field [V/m] and ρ is the electric charge density [C/m^3].

In the structural mechanics aspect of the simulation, the governing equations are based on the equations of linear elasticity and the equation of motion. These equations describe the deformation and motion of the motor's structural components under mechanical loads and stresses. The computed variable in this physics is the displacement vector field, denoted as u. Table 4.2 provides an overview of the governing equations for structural mechanics analysis in their differential form:

Equilibrium Equation	Generalized Hook's law	Compatibility Equation
$\nabla \cdot \sigma + f = \rho \frac{\delta^2 u}{\delta t}$	$\sigma = C\epsilon$	$\nabla \times \epsilon = 0$

Table 4.2: Governing equations for structural mechanics

where σ is the stress tensor, ϵ is the strain tensor, f is a force per volume unit [N/m^3], ρ is the mass density [kg/m^3], u is the displacement vector and C is the elastic tensor.

Boundary conditions and symmetry

As explained previously, by taking advantage of the symmetries inside the motor, we are able to drastically reduce the computational time required to solve the system. The simplification leads to the requirements of appropriate boundary conditions to correctly represent the complete motor behavior. We can divide the boundary conditions in two categories depending on the physics considered.

For the electromagnetism consideration, the motor sector is subjected to three different boundary conditions. Figure 4.3 illustrate their boundaries of influence.

- Magnetic insulation is applied on the stator outer surface and on the rotor inner surface. This approximation is valid as the casing around the motor and the motor shaft do not have significant influence on the magnetic distribution inside the motor.

- Boundary of anti-periodicity is applied on each side of the stator and rotor core to model the change in the magnetic periodicity of the motor. As we are centered on only one sector, the adjacent sectors have opposite polarity. This means that on the q-axis of the rotor, the magnetic flux is perpendicular to the boundaries.

- Sector symmetry is a tool available in *Comsol Multiphysics®* used to work with dynamic simulation when only one sector is modelled. This allows to rotate the rotor with respect to the stator and used a periodic conditions of antiperiodicity to model the next sector with opposite polarity when a relative movement of the rotor is used.

For the structural behavior, only the rotor model is solved. The rotor sector is also subjected to three boundary conditions. Figure 4.4 highlights their boundaries of influence.

- Free displacement is used on the rotor outer surface. This will help us to control the maximum displacement of the rotor when subjected to centrifugal effects assuring that we don't have contact with the stator element.
- Cyclic symmetry is applied on each side of the rotor core to simulate rotational symmetry. By dividing the motor into eight identical sectors, the cyclic symmetry boundary conditions assume that the behavior of the system in each sector is the same and that they are connected to form a closed loop. The azimuthal mode parameter, representing the number of discrete angular divisions or sectors in the system, is set to eight.
- Fixed boundary is used on the rotor inner radius to simulate a perfectly rigid attachment point with the fictive rotating shaft. This condition impose locally the displacement to be equal to zero.

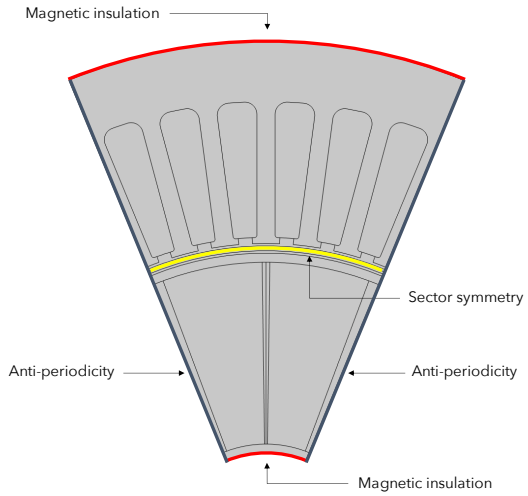

Figure 4.3: Boundary conditions: electromagnetism

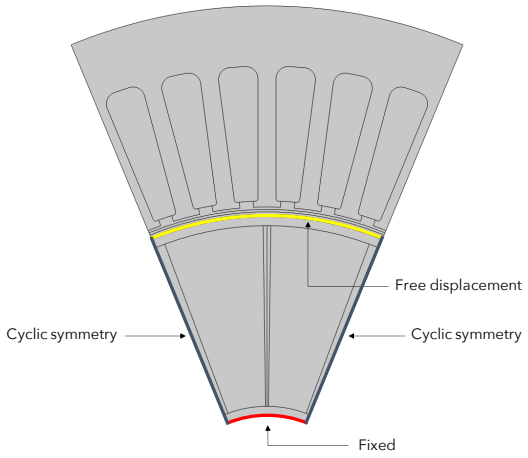

Figure 4.4: Boundary conditions: mechanics

4.1.3 Materials propreties

Given the limited data available on the current motor concept employed by *Formula Electric Belgium*, a decision has been made to use generic materials typically utilized in electric motors for EV applications. While specific details about the materials may be lacking, the selection of those generic materials provide a suitable foundation for conducting our study on the motor optimization.

Permanent magnets

Sintered Neodymium-Iron-Boron (NdFeB) magnets are considered in the motor design. The relevant material properties[1] are presented in Table 4.3.

Parameters	Values	Units
Relative permeability μ_r	1.05	/
Remanent flux density norm B_r	1.4	T
Density ρ	7500	kg/m^3
Young's Modulus E	160	GPa
Yielding strength S_y	200	MPa
Poisson ratio ν	0.24	/

Table 4.3: Permanent magnets properties

For the permanent magnets we can also add that:

- We do not consider the B-H characteristic of the permanent magnets.
- We do not consider limitation regarding permanent magnet demagnetization.
- We do not consider the thermal aspect affecting the permanent magnet performance.

Stator and rotor iron

The rotor yoke, stator yoke and stator teeth are modelled using a generic soft iron. While soft iron materials may not have particularly high mechanical strength or hardness, it has been chosen for its unique magnetic properties, including high magnetic permeability and low magnetic coercivity.

Parameters	Values	Units
Relative permeability μ_r	1200	/
Density ρ	7850	kg/m^3
Young's Modulus E	250	GPa
Yielding strength S_y	150	MPa
Poisson ratio ν	0.21	/

Table 4.4: Soft iron steel properties

Table 4.4 provides the soft iron properties employed for the optimization[2], while Figure 4.5 depicts the corresponding B-H curve of the soft iron material. It should be noted that the B-H curve is utilized only during the post-processing stage.

[1]The presented permanent magnets properties where obtained from the *Comsol Multiphysics®* and MagCam

[2]The presented iron properties where obtained from *Comsol Multiphysics®*

Throughout the optimization process, the analysis focuses on operating within the linear characteristic region of the material, where the relative permeability can be treated as constant. This assumption remains valid due to the chosen current density levels in the modeling, ensuring that magnetic saturation in the core material is not reached.

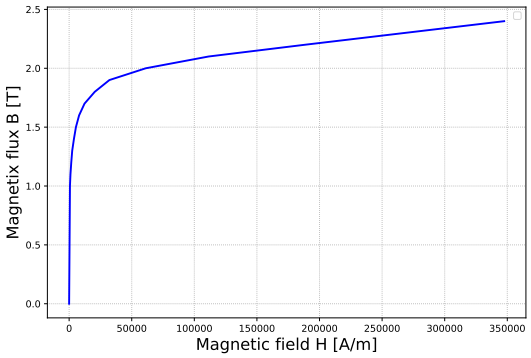

Figure 4.5: Soft iron B-H curve

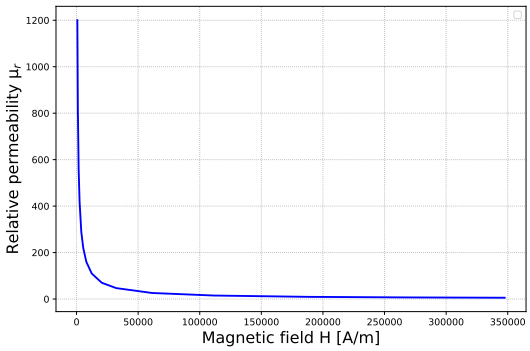

Figure 4.6: Soft iron μ_r

The relative permeability was deduce from the materials B-H curve as:

$$\mu_r = \frac{\Delta B}{\mu_0 \Delta H} \tag{4.1}$$

For the core of the machine, we can add that:

- We consider the B-H for the topology optimization as discussed above.
- We do not consider the thermal aspect impacting the B-H characteristic and the mechanical properties of the materials.

Windings

In the topology optimization phase, the stator windings are assigned the same material properties as air. This approximation is a commonly used in motor design and analysis. The rationale reason behind this approach is that the properties of the windings are not the most influential factors impacting the motor's performance.

The main purpose of the windings in an electric motor is to create a rotating magnetic field that interacts with the magnetic field produced by the permanent magnets. The windings are typically made of copper wires or other conductive materials that can carry electrical current. The electrical properties of the windings, such as their resistance or inductance, do have an effect on the motor's performance, but in most cases, these effects are relatively small compared to other factors such as the motor's physical design or the quality of the magnetic materials. By modeling the windings as having the same properties as the ambient air, we are essentially treating them as if they have no electrical resistance or inductance. This is a good approximation because it simplifies the analysis of the motor's performance without

significantly affecting the accuracy of the results. However, proper modelling of the windings is required when measuring losses and the overall efficiency of the motor.

The windings properties used in the modelling and optimization are referred in the following Table 4.5.

Parameters	Values	Units
Relative permeability μ_r	1	/
Electrical conductivity σ	0	S/m
Current density J	5	A/mm^2

Table 4.5: Windings properties

A constant current density of 5 [A/mm^2] was assigned for the optimization process. This is a typical value for a regime operation of an electric motor cooled by a water jacket. It guaranties a working condition in the linear region of the soft iron, avoiding magnetic saturation and excessive heating that can alter the materials properties and in term, the motor's performances.

4.2 Topology optimization study

Once the numerical model is defined, we can start the optimization study. Topology optimization methods are used to optimize the material distribution within a given design space to maximizing the performance of the system subjected to a set of constraints. It is a powerful tool for providing innovative and high-performance concepts at the early stages of the design process. Due to the free forms that naturally occur in the design space, the results of such optimization are usually difficult to manufacture, meaning the resulting design are often fine-tuned for manufacturability purpose.

The density-based topology optimization method is the most commonly used approach for solving optimization problems. In this method, the material of each element in the design is represented by a material density parameter, usually denoted as θ. There are two primary approaches for representing material densities: continuous densities and discrete densities.

Continuous densities refer to the use of a continuous variable to represent the density of one material in the design space. This approach allows for a smooth transition between different material densities, providing flexibility in optimizing the material distribution. However, it can result in more complex mathematical formulations and computational challenges.

On the other hand, discrete densities employ a finite number of discrete values to represent the density of a material. This approach simplifies the optimization

problem by reducing the number of possible material states, making it computationally efficient. One example of a discrete density method is the ON/OFF method, which was discussed in section 4.2. For this thesis, we will only focus on continuous density methods due to their flexibility in representing material distribution and their widespread usage in topology optimization problems.

In the context of continuous densities methods, Bendsøe and Kikuchi [7] proposed the Solid Anisotropic Materials with Penality (SIMP). This interpolation method involves representing the material distribution within the design space as a continuous function of a density parameter θ varying between 0 and 1. A density value of 1 indicates that the element is fully filled with material, while a density value of 0 indicates that the element is completely empty. The density of each element is used to interpolate between the material properties of the solid and void material. To force intermediate density values to either converge to 1 or 0, a penalty function is used. The penalization parameter, denoted as p, plays a crucial role in the SIMP method as it determines the level of material density in the final design. A higher value of p results in a more binary design with fewer intermediate densities, while a lower value of p results in a smoother, more continuous design. The choice of the penalization parameter is typically based on the desired level of details in the final design and the computational resources available. The penalisation function can take various forms, but a commonly used one is the power law:

$$\theta_p = \theta^p \tag{4.2}$$

In *Comsol Multiphysics®*, the penalized material volume factor uses a derivative of the power law and is expressed as follows:

$$\theta_p = \theta_{min} + (1 - \theta_{min}) \cdot \theta^p \tag{4.3}$$

where θ_p is the penalized material density and θ is the control density and θ_{min} is the minimum density value (fixed to 0.001). Figure 4.7 shows the relationship of the penalization parameter and the resultant density interpolation scheme.

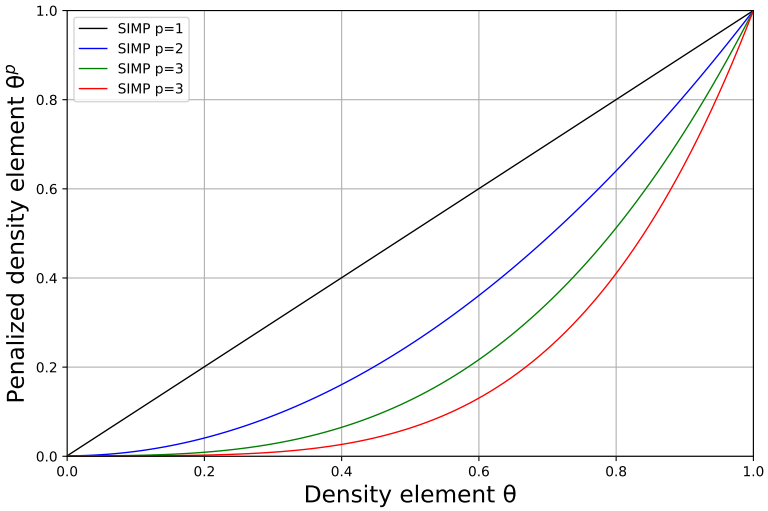

Figure 4.7: Penalization of intermediate densities in the SIMP model

To generate a complete model, the densities of all finite elements are unified into a single density field that represents the final material distribution within the design space.

The topology optimization problem is typically solved using gradient-based iterative algorithms, such as the Method of moving asymptotes (MMA). These algorithms are particularly suitable for differentiable and continuous objective functions. While other categories of optimization algorithms, such as derivative-free solvers, are usually used when the objective function is not computationally intensive.

Derivative-based optimization solvers are known for their efficiency and ability to handle complex problems with a large number of control variables. These solvers require relatively low computational time and are well-suited for complex optimization problems involving a large number of control variables. In the case of the MMA solver, the algorithm iterations update the density values of each finite element based on the sensitivity of the objective function to changes in density. These updates are made to improve the objective function value and optimize the design. The algorithm continues to iterate until sufficient convergence is achieved.

4.2.1 Filtering and projection in topology optimization

Although the SIMP method can yield satisfactory results on its own, additional processing methods can be employed to enhance the quality of the solution. One approach involves post-processing the raw control variable, denoted as θ_{raw}, obtained from the optimizer before it is penalized by the SIMP method. The post-processing step aims to refine the θ_{raw} variable by applying specific operations or filters to improve the resulting material distribution.

The density variables undergo two crucial processing steps before being penalized: filtering and projection. These processing steps introduce new parameters such as the filter radius and the projection slope in addition to the SIMP penalization parameter. The quality of the resulting topology solution is highly influenced by the values of these parameters. Figure 4.8 shows the processing scheme applied on each raw density control variable θ_{raw}.

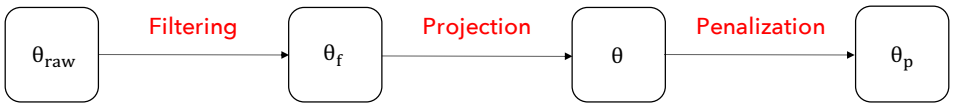

Figure 4.8: Processing of densities

To avoid potential numerical instabilities that can arise due to the lack of smoothness in the characteristic function, image processing-based filtering techniques are used in continuous based topology optimization. The density method in *Comsol Multiphysics®* supports a regularization technique known as the Helmholtz filter. This feature introduces a minimum length scale using the filter radius R_{min}:

$$\theta_f = R_{min}^2 \nabla^2 \theta_f + \theta_{raw} \tag{4.4}$$

where θ_{raw} is the raw density, modified by the optimizer and θ_f is the filtered density. By default, the filter radius is set to the average size of the mesh edges. This works well in terms of regularizing the optimization problem, but it's important to set a fixed radius larger than the mesh edge size to get mesh-independent results. To address this concern, the filter radius, is set to the coarser mesh element size.

The outcome density field of the Helmholtz filter gives rise to a grayscale image. Interpreting and analyzing the grayscale image can be challenging due to its continuous nature. To facilitate a more intuitive representation, a projection method is applied to reduce the grayscale to a more binary or discrete form. A commonly used projection technique is based on a hyperbolic tangent function. The amount of projection can be controlled through the projection steepness parameter β:

$$\theta = \frac{\tanh \beta(\theta_f - \theta_\beta) + \tanh \beta\theta_\beta}{\tanh \beta(1 - \theta_\beta) + \tanh \beta\theta_\beta} \tag{4.5}$$

where θ_β is the projection point of θ_f. The projection steepness is left as default during the optimization. Figure 4.9 and 4.10 illustrate the processing of the densities in the context of the structural optimization of a beam [25].

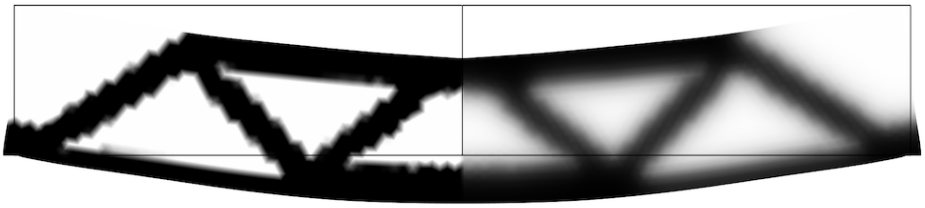

Figure 4.9: Illustration of a raw density field to the left and the corresponding filtered field to the right. [25]

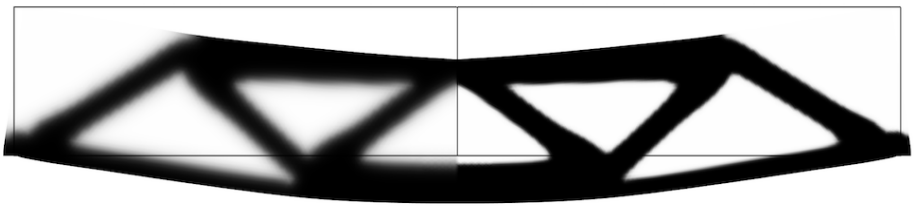

Figure 4.10: Illustration of a filtered field to the left and the corresponding projected field to the right. [25]

Finally, the resulting control variables provided by projection are penalized with the SIMP method to force intermediate values to converge either to 0 or 1. The value of the SIMP exponent is one of the most important parameters in term so results quality. Two approaches can be taken when using the SIMP penalization:

- Continuous penalization method: this method consist of increasing the value of the penalization exponent progressively during the optimization. This technique is usually used for complex problems where there might be many local minima in the solution space. The solver will ramp over the penalization exponent, starting from a low to higher values. The method can be extended to other parameters such as the minimum filter radius or projection slope parameter.

- Standard penalization method: this method consist of maintaining the value of the penalization exponent constant during the complete optimization. The quality of the solution depends on its complexity.

Both methods were tested at the early stage of the optimization process and the results obtained where very similar. Considering the additional computational time and complexity associated with the continuous penalization method, it did not demonstrate a significant advantage that warranted its adoption for our study. As a result, the standard penalization method was chosen as the preferred approach for our case.

To determine the optimal values of the SIMP exponents for the defined densities, a sensitivity analysis was conducted. This analysis consist of running multiple times the same simulation with varying values of the exponents and analyzing the resulting designs and objective function to identify the most suitable composition of the penalization. This sensitivity analysis played a crucial role in fine-tuning the SIMP method to obtain the most efficient designs.

4.3 Electromagnetic Torque Characteristics

There are multiple methods based on finite element solutions which can be used for calculation of electromagnetic torque of PM synchronous machines. Some common approaches are:

1. Maxwell Stress Tensor

2. Arkkio's method

In depth comparative analysis of accuracy between the above methods can be found in [21]. In this thesis, the magnetic torque will be computed using both methods. Although the Maxwell Stress Tensor is generally regarded as more accurate, it requires significantly higher computational resources. Consequently, Arkkio's method will be utilized for evaluating torque performance during the topology optimization process, where computational efficiency is of great importance. Once the topology optimization process is complete, and the final design is obtained, the Maxwell Stress Tensor will be applied for a detailed analysis and comparison with the reference motor.

4.3.1 Torque contribution

One of the main advantage of IPM designs is their high saliency ratio (L_q/L_d). The high value of this ratio allows the motor to take advantage of both the magnetic and reluctant torque component. The motor torque that derives from the interaction between the armature current[3] and the permanent magnet flux can be written as follows.

$$\begin{aligned} T_{em} &= \frac{3}{2}p[\phi_m i_q + (L_d - L_q) i_q i_d] \\ &= \underbrace{\frac{3}{2}p\phi_m i_q}_{\text{magnetic torque}} + \underbrace{\frac{3}{2}p(L_d - L_q) i_q i_d}_{\text{reluctant torque}} \end{aligned} \tag{4.6}$$

Where p is the number of poles, ϕ_m is the flux linkage, i_q and i_d are respectively the current in the q- and d-axis, L_q and L_d are the inductance along the q- and d-axis respectively. We can see that the motor torque can be broken down in the two components: magnetic torque and reluctance torque.

The magnetic torque is originated from the Lorentz force, due to the interaction between the magnet's flux field and the current in the stator windings.

On the other hand, the reluctant torque component originates from the difference between the d- and q- axis inductance of the rotor. The reluctant force can be seen as the force acting on the magnetic material that tends to align with the main flux to minimize reluctance.

From the torque equation 4.6, we can see that both component of the torque are solicited for a specific angle of excitation. The angle of excitation refers to the phase angle between the stator voltage and the rotor flux vector. In a phasor diagram, it is the angle between the rotor d- axis and the instantaneous stator winding phasor. It is also known as the electrical phase angle ϕ_e. Figure 4.11 shows the phasor representation of the system where θ_m is the mechanical angle of the rotor.

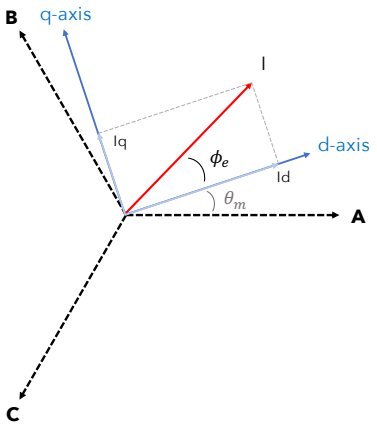

Figure 4.11: Phasor system representation

We can observe from equation 4.6 that each torque component are maximized at different values of the rotor axis currents. The magnetic torque is maximized when the stator field excites the rotor 90 electrical degrees from the d- axis, i.e when the

[3] Stator currents

current i_q is maximum. On the other hand, the reluctance torque follows a different path and is maximized at 45 electrical degrees past the q- axis, i.e. when i_d and i_q are equal. The maximum magnetic torque takes advantage of both the motor's reluctance and magnetic torques contribution. Shifting further away from the q-axis reduces magnetic torque, but is far outweighed by the gain in reluctance torque. The maximum combination of the magnetic and reluctance torque theoretically occurs near the 45 electrical degrees from the q axis, but the exact angle will vary based on the characteristics of the PM motor. Figure 4.12 represents formally the contribution of the two torque components with respect to the electrical phase angle. In this image, an current phase angle of 0[°] correspond to the aligned of the current phasor and the rotor q- axis.

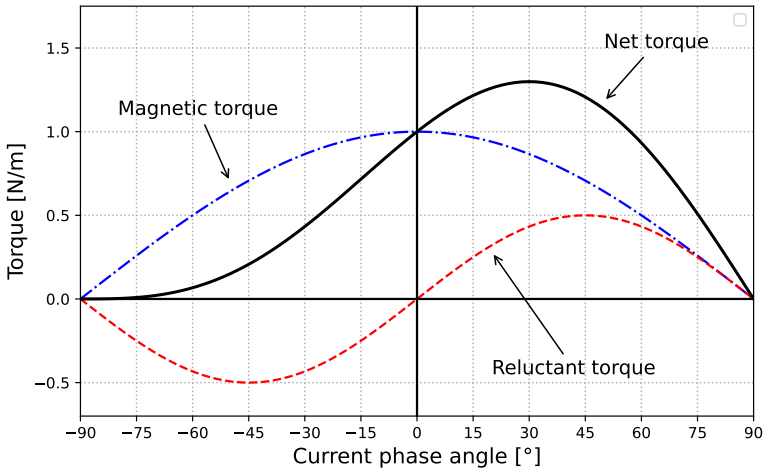

Figure 4.12: Torque components

Figure 4.12 highlights the intimate link between the rotor design, hence the salicency ratio (L_d/L_q) and the performance of the motor. During the topology optimization of the rotor, we will leave the electrical angle as a design parameter, meaning that the solver has the degree of freedom to distribute the torque contribution between the two component (magnetic and reluctant) as it pleases. This will allow to find the optimum combination of L_q, L_d and the values of i_d and i_q.

4.3.2 Torque Ripple

The torque ripple refers to the periodic oscillations of the electromagnetic torque arising during operation in electric motors. This parameter is very important regarding the overall performance of the motor. The torque ripple is measures as follows:

$$T_{ripple} = \frac{T_{max} - T_{min}}{T_{avg}} \tag{4.7}$$

where T_{max} and T_{min} are respectively the maximum and minimum torque measured over one electrical period and T_{avg} is the average motor torque. In a PM machine, the torque ripple can originate from the following factors [22] [23]:

- Cogging torque: The cogging torque originates from the interaction between the permanent magnets and the teeth of the stator slot openings and is normally independent of any excitation in the stator windings. The amplitude and frequency of the cogging torque depends on the LCM of the number of slots and rotor poles. In general, higher the value of the LCM is, the lower the cogging torque contribution. The cogging torque amplitude is inversely proportional to the number of cogging torque periods N in a rotor revolution. The cogging torque period can be expressed as:

$$N = LCM(n, p) \tag{4.8}$$

  where n is the number of slots and p the number of poles. Thus a high value of N is desirable to decrease the amplitude of the cogging, while increase the periodicy of the signal. In our machine design, the number of slots is equal to 48 and the number of poles is 8, resulting in a LCM of 48. This value of LCM is relatively high for the very compact size of the motor.

- Non-ideal back-EMF waveforms: Back-EMF voltage is induced in the stator windings due to the relative movement of the rotor magnetic field and the stator. The waveform of this induced voltage is usually not sinusoidal and highly depends on the geometric design. This means that the back-EMF has harmonics that interfere with the torque production of machine, leading the torque ripple.

- Magnetic saturation: The saturation of the machine's magnetic circuit is a less common source of torque ripple since the saturation of materials is almost always avoided in the design because of the additional problems that it brings. Saturation may increase torque fluctuations because of the non-linear magnetic behavior of the material in these conditions. During saturation, the airgap flux density distribution is affected, and since airgap flux density is directly related to torque, higher fluctuations appear.

- Mechanical asymmetries: Asymmetries in the rotor and stator, such as uneven air gap, manufacturing tolerances, and eccentricity, can cause variations in the magnetic field, resulting in torque ripple.

During the design and modelling of the PM motor, it is assumed that the motor is supplied by perfectly sinusoidal currents. However in reality, the inverter output current contains ripple which give rise to time harmonics in the supply currents. This combination with space harmonics of air gap field can cause additional torque ripple. The torque ripple contribution that we are effectively measuring from the FEM modelling of the motor is the cogging component.

Motor dynamics

As we have discussed, the torque ripple is an important design performance that will highly influence the quality of the motor. Thus, a low value of ripple is desired.

Nonetheless, for some motors, high torque ripple can still be acceptable and will not be a severe issue. In fact it is important to study the dynamic behavior of the system as a hole. Equation 4.9 expresses the equation of motion for an electric motor. It quantities the variations of speed on the rotor shaft due to electromagnetic torque ripple. We can see that the rotational inertia of the system can filter the speed variation of the rotor. This shows that the inertia of the system has to be considered before concluding on the ripple quality of the system.

$$T_{em} - T_r - K_v \cdot \omega = J_m \frac{d\omega}{dt} \tag{4.9}$$

where T_{em} is the electromagnetic torque [Nm], T_r is the resistive torque due to mechanical friction in the rotating system [Nm], K_v is the viscous friction coefficient [Nms], ω is the rotating speed [1/s] and J_m is the moment of inertia of the assembly (composed of the motor and the load)[Nms^2].

4.4 Mechanical Analysis of PMSM

In addition to the magnetic analysis, a mechanical study is conducted to ensure the structural integrity of the machine during operation. However, since the primary focus of this study is the optimization of the rotor topology, the discussion will mainly revolve around the sources of stress that affect this rotating component.

It is important to note that the stator is also subjected to mechanical stress originating from various sources. For instance, the stator experience stress due to the thermal expansion of the material as a result of the heat generated during operation. Additionally, the magnetic forces within the system can exert high stresses on the stator teeth elements. While the mechanical analysis of the stator is beyond the scope of this particular study, it is acknowledged that a thorough investigation of its mechanical behavior would be essential for future research and development of the motor.

The mechanical analysis of the rotor aims to evaluate the stress distribution, the identification of potential failure points, and the determination of the optimal rotor design to withstand the anticipated mechanical loads. This section will first discuss the failure theory considered for the mechanical analysis and will be followed by an exhaustive list of the sources of stress acting on the system.

4.4.1 Material yielding and failure theory

To study the mechanical stresses in a rotating machine, it is crucial to have a thorough understanding of the mechanical behavior of materials under various loading conditions. A body can be subject to volume forces and/or a surface forces.

Volume forces are the result of a force fields, such as gravity, which act on the entire volume of the body. These forces result in a distribution of stress within the material. In the context of a rotating machine, the primary volume force

is the radial centrifugal force. As the rotor rotates, the centrifugal force acts radially outward from the center of rotation, creating a volumetric load on the rotor materials.

Surface forces, on the other hand, are forces applied directly to the surfaces of the body through contact with other bodies or components. In the case of a rotating machine, the surface loads primarily arise from the internal magnets pushing on the iron core due to the centrifugal effect. These forces can cause localized stresses on the surface of the rotor, which need to be analyzed and considered for ensuring the structural integrity of the rotor.

Materials can be classified into two categories based on how they deform and respond to the applied forces. We can distinguish ductile materials and brittle materials.

- Brittle materials: Brittleness is a mechanical property that describes a material that have limited deformation capability and tend to fracture at lower strains, rather than deforming or bending. Brittle materials do not exhibit significant plastic deformation before failure. A very common example of brittle materials used in the motorsport industry are carbon fibers composites.

- Ductile materials: ductility is the mechanical property that describes a material's ability to deform under loading, without breaking or fracturing. These materials can absorb energy by undergoing significant plastic deformations before they fail, which makes them suitable for many applications where the material is subjected to repetitive or cyclic loading.

Given the requirements and considerations for rotor applications, it is evident that ductile materials are more suitable. Therefore, in this study, the focus will primarily be on ductile materials, particularly iron, due to its high presence in the rotor core.

The stress-strain relationship, which describes the correlation between external forces or stresses (σ) applied to a material and its resulting deformation or strain (ϵ), is represented in a typical stress-strain diagram. These relationships, also known as constitutive equations, encapsulate the material properties of the body. Figure 4.13 illustrates a typical stress-strain curve obtained from subjecting a ductile material to a uni-axial load. However, the stress-strain behavior of the material is often approximated omitting the lower and upper yielding points. Figure 4.14 provides an illustration of a simplified characteristic curve that approximates the real stress-strain relationship.

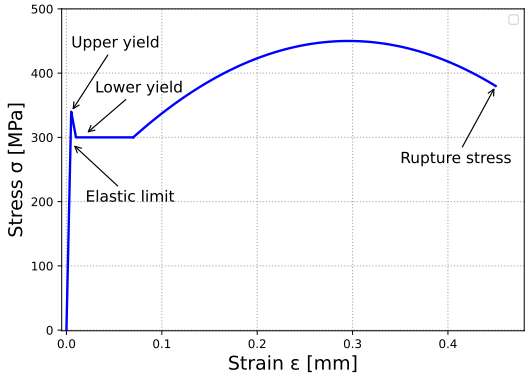

Figure 4.13: Typical σ-ϵ curve

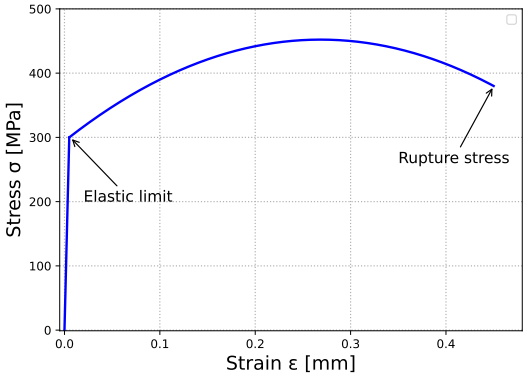

Figure 4.14: Simplified σ-ϵ curve

From these figures, we will distinguish three important concepts:

- The elastic limit: The elastic limit defines the region where energy is not lost during the process of stressing and straining. That is, the processes that do not exceed the elastic limit are reversible. In the elastic region, the stress evolves linearly with the strain. The elastic limit is also called yield strength S_y. Above that limit, the deformations stops being elastic and start being plastic, including irreversibly.

- The upper and lower yield: when the material is deformed and reaches the critical point, called the upper yield limit, the stress will drop rapidly to the lower yield limit from where a constant characteristic can be observed until the material starts resisting the deformation again. The lower yield is usually neglected and we only consider the upper yield.

- The rupture stress: the rupture of fracture point is reached when large deformation are applied in the material plastic region. When reaching the rupture point of the material, a sudden breaking can be expected. Materials that have the property of fracturing only after large plastic deformations are called ductile.

During the design process, it is crucial to ensure that the operating conditions of the rotating machine remain within the elastic region of the material, avoiding yielding. This conditions must be assured particularly at maximum rotating speed, where the centrifugal stresses are at the highest.

Failure theory : maximum elastic distortional energy criterion

In order to predict and prevent the conditions of ductile failure, the von Mises criterion, also known as the maximum elastic distortional energy criterion, will be employed. This criterion is commonly utilized to assess the yielding behavior of ductile materials under complex loading conditions.

The von Mises criterion is formulated under the von mises equivalent stress or equivalent tensile stress σ_v. This theoretical value allows the comparison between

the overall tridimensional stress state and the yield limit of the material under uni-axial stress conditions. A material is said to start yielding when the von Mises equivalent stress reaches the yielding strength of the material. The criterion is written as follows:

$$\sigma_v \leq S_y \tag{4.10}$$

Detailed computation regarding the von Mises equivalent stress is out of the scope of the thesis but more informations can be found in [24].

During the design of the new rotor, the von Mises yield criterion must be respected to assure the structural integrity of the rotor in the harshest operation condition. Additionally, the rotor can be designed with a high safety factor to prevent even more mechanical failure. In the automotive industry the safety factor SF typically lies in between (1.2 and 1.4). The critical yielding criterion that will be used is expressed as follows:

$$\sigma_v \leq \frac{S_y}{SF} \tag{4.11}$$

4.4.2 Mechanical stresses acting on the rotor

The rotor of a permanent magnet machines is subjected to a variety of stresses during operation, which can affect the performance and reliability of the machine. The main mechanical stresses arise from centrifugal effects, magnetic forces, thermal expansion and tangential forces.

Centrifugal force is the major source of mechanical stress acting on the rotor. This force is the apparent outward force acting on a mass when it is rotated and is evolving quadratically with the rotational speed. This source of stress causes the rotor to deform and elongate especially at high speed. In term the deformation can result in high stress concentration regions and lead to cracking or even failure of the rotor, causing severe damage or even total disintegration of the complete motor. In addition, if the elongation of the rotor is too high, it could enter in contact with the stator, compromising the integrity of the assembly. Figure 4.15 illustrates the volume load due to centrifugal effects on a generic rotor sector. This volume force can be formulated as:

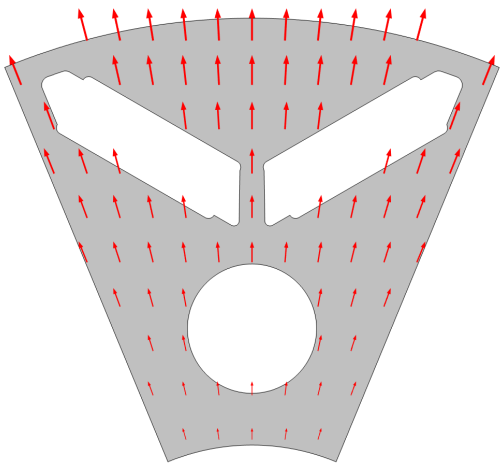

Figure 4.15: Centrifugal loading

$$F_c = m \cdot \omega^2 \cdot R \tag{4.12}$$

An important aspect to consider is that the rotor is not only subject to its own body load, but has to manage the surface forces exerted by the retained internal permanent magnets. We will see in subsection 5.1.2 how this load contribution is taken into account during the topology optimization of the rotor. Figure 4.16 illustrates the contact force due to the PM on a generic rotor sector.

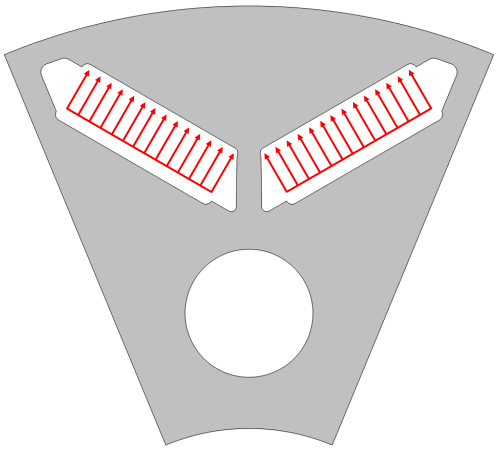

Figure 4.16: Contact force due to the permanent magnets

While the centrifugal force is acting radially on the rotor part, a tangential force arise due due to the rotor's own inertia. This force component is mainly affecting the core during transient operation, meaning when the motor accelerates or decelerate. The tangential force is directly related to the moment of inertia of the rotor and the angular acceleration. According to Newton's second law of motion for rotational motion, the tangential force F_t can be calculated using the equation:

$$F_t = I\frac{d\omega}{dt} \tag{4.13}$$

where I represents the moment of inertia of the rotor and ω represents the angular speed. This force contribution can become dominant for very short periods of time, during extreme throttling of the motors.

Finally, as mentioned earlier, rotors are also subjected to other sources of mechanical stresses such as magnetic forces and thermal expansion.

The magnetic forces originates from the interaction between the rotor's permanent magnet and stator magnetic field. This force is responsible for producing the torque that drives the rotation of the rotor. The magnetic force is not tangential to the rotor's motion but rather acts perpendicular to the magnetic field lines.

The thermal expansion originated from the thermal expansion properties of the rotor and stator materials. The machine usually heats up at higher load and

rotating the speed due to the increase of the copper and iron losses resulting in an increase of dissipated heats rejection.

These two stress sources are not taken into account during the design process, having less important on the overall loading of the motor.

5 | Design and optimization

This chapter describes the optimization and design phase of the project. We will formally define the topology optimization problem and present the out-coming configurations. After that, we will compare the new topologies using a three-objectives pareto front. From those results, we will form the final solution by post-processing the optimal resulting topology and finally perform a comparison with the reference motor design.

5.1 Topology optimization

As explained in the research approach and methodology of this study, the topology optimization is used to explore multiple sets of designs. The sets are characterized by a fixed rotor mass and are composed of eight topologies. Within each set, the topologies differ in terms of the ratio between the permanent magnet and iron materials used in the rotor. This approach serves multiple objectives:

1. Find the optimum distribution between iron and permanent magnets composing the rotor.
2. Observe the impact on the performance of the iron quantity forming the core.
3. Find an optimum topology for the rotor.

During the optimization, four sets of optimize topologies were formed with the following masses:

15% mass reduction	$m_{rotor} = 0.85$ [kg]
20% mass reduction	$m_{rotor} = 0.80$ [kg]
25% mass reduction	$m_{rotor} = 0.75$ [kg]
35% mass reduction	$m_{rotor} = 0.65$ [kg]

Table 5.1: Constraint rotor masses used during the topology optimization

It is important to recall that the reference motor yields a rotor mass of 1[kg].

5.1.1 Problem formulation

The optimization aims to maximize the average torque of the design. The objective function can be formulated as follows:

$$\boxed{\min \sum_{i=0}^{n_{sol}} \frac{-T_i}{n_{sol}}} \tag{5.1}$$

and the design must respect the following constraints:

$$\text{subjected to } S < 1,\ m_{PM} < \alpha_1 \text{ and } m_{iron} < \alpha_2$$

To approximate the average torque, we evaluate at each optimization step the instantaneous torque T_i for n_{sol} rotor positions. The average is than taken. The problem has also three constraints:

- $S < 1$ assures that the maximum equivalent stress in the topology is below the iron yielding point. The parameters S is defined as:

$$S = \frac{\max(\sigma_v)}{\frac{S_y}{SF}} \tag{5.2}$$

  with S_y is the iron yielding strength, SF a safety factor of 1.25 and σ_v von Mises equivalent stress.

- $m_{PM} < \alpha_1$ and $m_{iron} < \alpha_2$ constraint the maximum mass of permanent magnets and iron in the design and in term, in term constraining the maximum mass of the rotor. The coefficient α_1 and α_2 are obtained based on the desired rotor mass.

5.1.2 Density definitions

As explained in the previous chapter, the densities are the control variables of the topology optimization. In our study, they act on two kinds of materials proprieties: magnetic properties and mechanical properties. The penalized control densities θ_p are defined as follows:

Material or property	Density indice
Permanent magnet or Iron	$\theta_p^1 \in [0{:}1]$
Remanent flux orientation	$\theta_p^2 \in [0{:}1]$
Electrical phase angle	$\theta_p^3 \in [0{:}1]$
Material or void	$\theta_p^4 \in [0{:}1]$

Table 5.2: Densities definitions

As discussed in subection 4.1.2, the sector geometry is designed to be centered on the d-axis. This choice allows us to exploit the inherent symmetry within the rotor pole, effectively reducing the complexity of the problem. In Figure 5.1, the

design space for optimization is illustrated, along with the defined sub-regions.

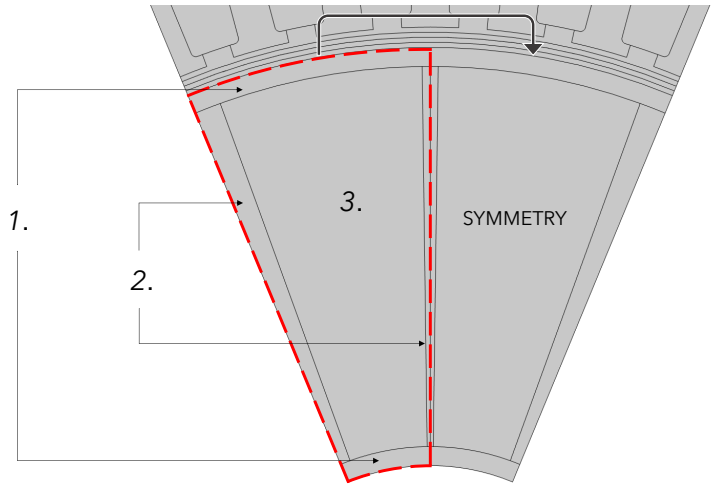

Figure 5.1: Rotor design space: divisions into sub-domains

To streamline the optimization process and minimize computational time, the rotor sector is initially divided into two domains: the left and right domains. In Figure 5.1, the left design domain is highlighted in red. The optimization problem is solved on one of these domains, and the properties computed for that domain are mirrored to the corresponding region on the other side. This approach significantly reduces the number of nodes to be solved at each optimization steps.

Furthermore, within the sub-design domain, three distinct design regions are defined. These regions enable a more targeted optimization approach, allowing for specific modifications to be made in different areas of the rotor sector.

- Region 1: in this region, not densities are defined and the material used by default is iron. For the upper part, this was done to assure that the magnets are buried inside the rotor core. On the lower portion near the shaft, this approach was used to assure having a minimum quantity of iron to allow the integration on the power transmission. We will see during the final results analysis that this region is obsolete and can be removed.

- Region 2: in this region, density θ_p^1 is not defined. This means that the solver can place either iron or air. The objective is to assure the structural integrity of the rotor, avoiding that the whole span of the sector is filled with magnets.

- Region 3: in this region, all densities are defined. This means that the solver can place either iron, permanent magnets or air.

By leveraging the symmetry of the rotor geometry and implementing the sub-regions, we are able to optimize the design more efficiently, achieving significant computational time reduction.

In the next part of this section, the notation x^y denotes that the material property x is defined in region y.

Materials magnetic properties

The optimization solver has the freedom to dispose permanent magnets, iron and air within the designated design space. The SIMP method is utilized to control the material permittivity ν. From a try and error process, it has been demonstrated that acting on the material's permittivity rather than the material's permeability, μ, offers improved convergence rates.

In addition to optimizing the materials distribution, the electrical phase angle of the three phase system and the orientation of the remanent flux of the permanent magnets are also optimized. The interpolation schemes used to represent each optimized quantity are defined as follows:

Materials permittivity

$$\nu_p^1 = 1 + \theta_p^4 \cdot (1 - \theta_p^1) \cdot (\nu_{iron} - 1)$$
$$\nu_p^2 = 1 + \theta_p^4 \cdot (\nu_{iron} - 1)$$

we assumed as approximation that the permittivity of the permanent magnets is equal to the one of the air ($\nu_{PM} = \nu_{air} = 1$).

Permanent magnets remanent flux

$$Br_p = Br_{pm} \cdot \theta_p^4 \cdot \theta_p^1$$
$$Brx_p = \cos\left(\theta_p^2 \cdot \frac{\pi}{180}\right) \in [0:1]$$
$$Bry_p = \sin\left(\theta_p^2 \cdot \frac{\pi}{180}\right) \in [0:1]$$

where Br_p is the magnitude of the remanent flux density, Brx_p and Bry_p are respectively X and Y components forming the base vector of the remanent flux density orientation expressed in the Cartesian frame of reference.

Electrical phase angle

$$\phi_{e,p} = (1 - \phi_{max}) \cdot \theta_p^3 + \theta_p^3 \cdot \phi_{min}$$

where the maximum electrical phase angle $\phi_{max} = 180[°]$ and the minimum electrical phase angle $\phi_{min} = 0[°]$. In this case, a phase angle of $0[°]$ represents an alignment of the three-phase phasor with the rotor d-axis, while a phase angle of $90[°]$ represents an alignment of the three-phase phasor with the rotor q-axis. This degree of freedom of the optimizer allows the optimum distribution between the d- and q- axis current, maximizing the performance as explained in 4.3.1.

Materials mechanical properties

To incorporate the structural mechanics of the design, the Young's Modulus E and material densities ρ are interpolated. In this study, a specific assumption is made regarding the stress distribution in the design. It is assumed that only the rotor iron core contributes to stress reduction, while the permanent magnets are omitted to contribute to the minimization of the centrifugal stresses. As a result, the Young's Modulus of the permanent magnets is set to zero, indicating that they are not actively contributing to stress reduction.

To take in consideration the contact forces between the permanent magnets and the iron core, the material densities ρ_p^i take into account the contribution of the permanent magnets.

Young's Modulus

$$E_p^1 = \theta_p^4 \cdot (1 - \theta_p^1) \cdot E_{iron}$$
$$E_p^2 = \theta_p^4 \cdot E_{iron}$$

Densities

$$\rho_p^1 = \theta_p^4 \cdot (1 - \theta_p^1) \cdot \rho_{iron} + \theta_p^1 \cdot \rho_{pm}$$
$$\rho_p^2 = \theta_p^4 \cdot \rho_{iron}$$

This approach provides a thoughtful method to consider the surface load of the permanent magnets while simultaneously aiming to minimize the stresses exerted on these components.

5.2 Results of optimization

5.2.1 Results: rotor shape analysis

Figure 5.2 represents the resulting topologies obtained from the different sets of optimized rotor masses. For the purpose of visualization, the following figure was placed horizontally. This allows to reach this comparison along its two main axes: for a fixed rotor mass, with varying $\frac{m_{PM}}{m_{TOT}}$ ratio and for a fixed $\frac{m_{PM}}{m_{TOT}}$ ratio, with different rotor masses. This visual representation allow us to identify certain patterns and trends arising in the distribution of the materials.

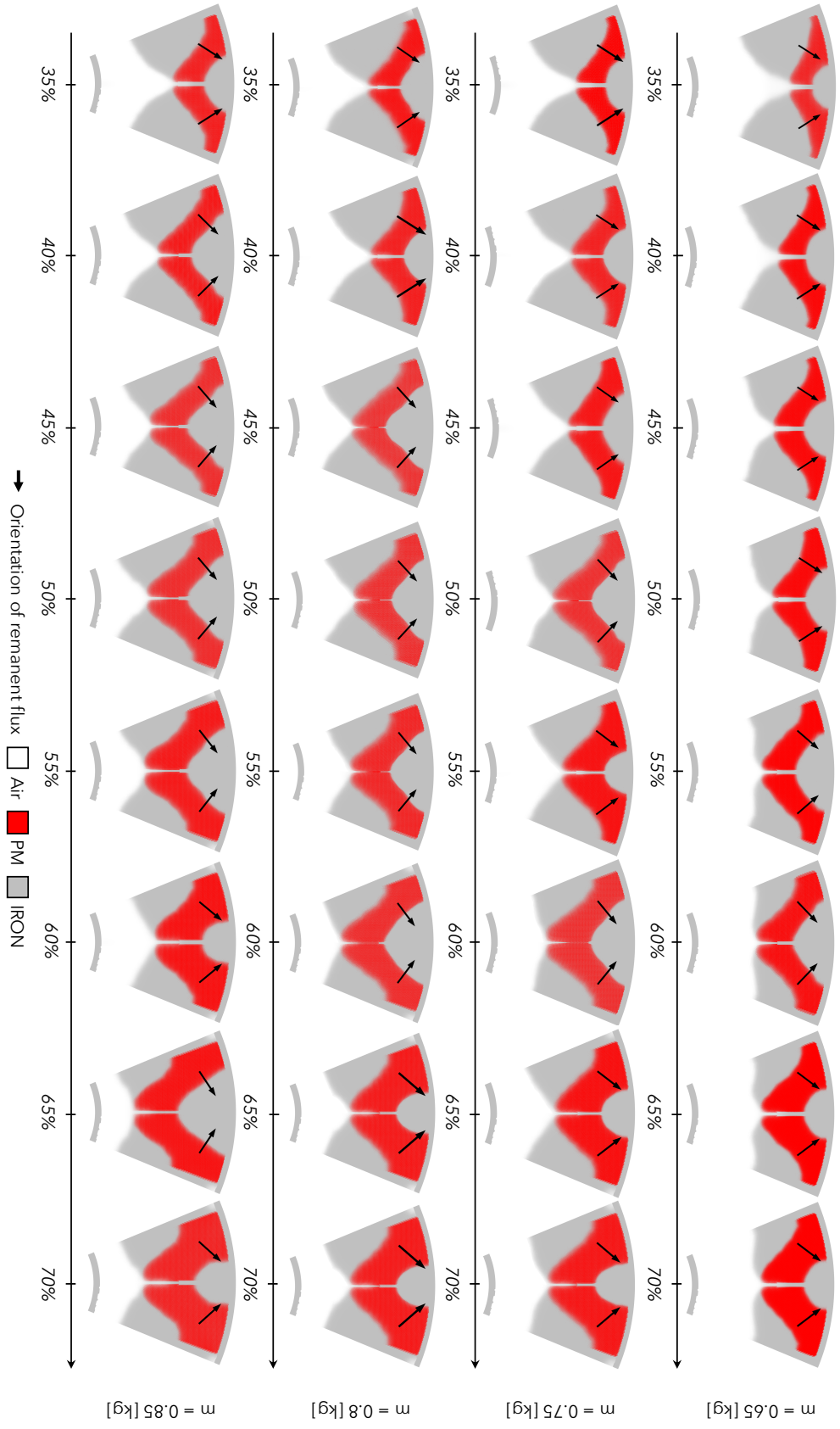

Figure 5.2: Topology sets with the ratio $\frac{m_{PM}}{m_{TOT}}$ expressed in %

- Permanent magnets: the permanent magnets are disposed in a reassembling V-shape. We can observe that increasing the magnet quantity does not significantly affect their disposition. For a lower magnet quantity, we can see that the solver tends to spread out the magnetic pole on the hole span, resulting in a bigger V-angle[1]. On the other hand, the magnets have smaller V-angle when increase the mass ratio.

- Rotor iron core: the main pattern that emerges in the presented results is the division of the rotor design space into two distinct regions. The optimizer removes the iron material in the lower part of the rotor, particularly in proximity to the connection with the shaft. This observation suggests that the iron material in this specific region is not essential for torque generation in the motor. This is a promising observation in terms of reducing the overall weight of the rotor without compromising its performance. Additionally, we observe that the distribution of the remaining iron material follows the path of the magnetic flux generated by the magnets. This alignment of the iron material with the flux path indicates a deliberate arrangement to optimize the motor's magnetic circuit. It is noteworthy that the pattern of the iron material remains relatively consistent across the various optimized topologies, suggesting the presence of an optimal configuration.

- Direction of the remanent flux: the orientation of the magnets field exhibits a slight inward turning when the mass ratio is increased. When the quantity of magnets is lower, the optimizer tends to distribute the magnetic poles over a larger span. In contrast, when the quantity of magnets is higher, the optimizer tends to concentrate the magnetic poles by burying more the magnets inside the core. Although this observation may not be as pronounced or easily discernible, it still holds potential value for the subsequent steps of the optimization process.

5.2.2 Results: performance evolution

Based on the different topology sets, we can draw the evolution of the average torque with respect to the mass ratio $\frac{m_{PM}}{m_{TOT}}$. Figure 5.3 represents this evolution where the average torque is evaluated over one electrical period.

[1] the V-angle being the angle between the vertical axis and the longitudinal dimension of the magnet

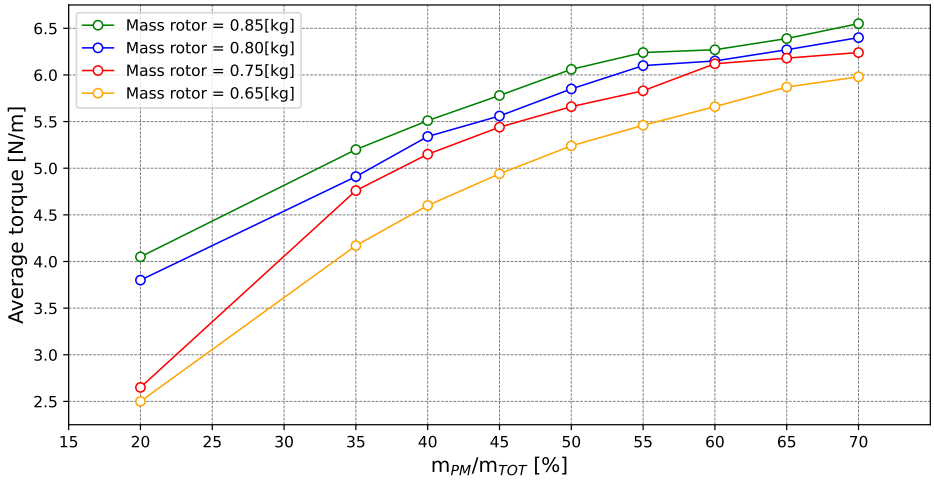

Figure 5.3: Evolution of the torque average for the different topology set

One evident and expected observation is that the average torque exhibits a consistent increase with the quantity of permanent magnet material in the rotor design. It is worth noting that the torque curves tend to reach a plateau at around the 70% mark ratio.

Additionally, a clear relationship can be recognized between the rotor mass and the average torque as the curves maintain a similar spacing between them. On average, an increase of 0.2 [Nm] in average torque can be observed for every 50 [g] increase of rotor mass.

5.2.3 Derived Pareto fronts

Reference data points

Before comparing the results of the topology optimization, it is essential to establish the data points for the reference model. The reference rotor performance serves as the baseline for the Pareto analysis. These data points are obtained through a multi-objective parametric optimization process[2].

The optimization aims to maximize the average torque while minimizing the torque ripple [3]. The reference model optimization problem can be formulated as follows:

$$\min \left[\frac{\alpha}{w_1} \sum_{i=0}^{n_{sol}} \frac{-T_i}{n_{sol}} + \max[\frac{(1-\alpha)}{w_2} \cdot (T_i - \sum_{i=0}^{n_{sol}} \frac{T_i}{n_{sol}})^2] \right] \tag{5.3}$$

[2]The parametric optimization in this study employed the BOBYQA (Bound Optimization By Quadratic Approximation) solver. This is a derivative-free optimization method widely used for solving constrained optimization problems. The BOBYQA solver approximates the objective function using quadratic models and iteratively explores the parameter space to find the optimal solution.

[3]In this case, the formulation for the torque ripple differs from the theoretical definition of the ripple value. This is simply due to limitations in the software implementation.

where $\alpha \in [0{:}1]$ is used to weight the objectives and obtain the reference Pareto front, while w_1 and w_2 are used to normalize the multi-objective function. In addition, the design must respect the following constraint:

$$\text{subjected to } S < 1,\ S_{PM} = S_{ref,PM}$$

As explained previously, to approximate the average torque we evaluate at each optimization step the instantaneous torque T_i for n_{sol} rotor positions. The average value is than taken. The problem has also two constraints:

- $S < 1$ assures that the maximum equivalent stress in the topology is below the iron yielding point of the material. The parameters S is defined as:

$$S = \frac{\max(\sigma_v)}{\frac{S_y}{SF}} \tag{5.4}$$

  with S_y is the iron yielding strength, SF a safety factor of 1.25 and σ_v von Mises equivalent stress.

- $S_{PM} = S_{ref,PM}$ constraint to used the same magnet quantity as used in the reference concept currently used by the team ($S_{ref,PM} = 82.2$ [mm^2]).

In the multi-objective optimization process, the rotor mass is kept constant, while only the geometric dimensions and the position of the permanent magnets are varied to explore different spoke configurations.

Pareto optimal

The following figures represent a multi-objective Pareto analysis comparing the three main design performances: the average torque, the torque ripple and total mass of the rotor. For comprehension purpose, Figures 5.4, 5.5 and 5.6 focus on different 2D perspectives of the 3D Pareto front. The data points from the reference model were found as presented in 5.2.3.

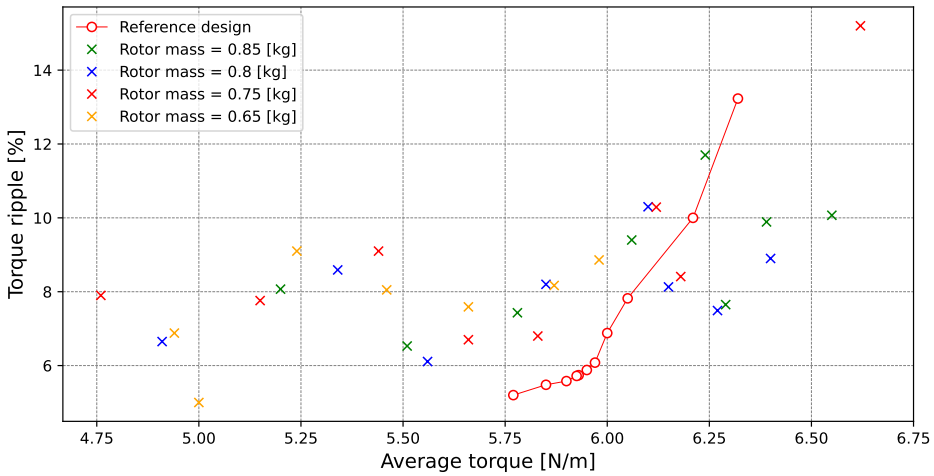

Figure 5.4: Average torque and torque ripple

From Figure 5.4 no clear patterns appear in the topology optimization results when considering the torque ripple. This is simply due to the limitation that our optimization study does not take the torque ripple as an objective function. This limitation will be further discussed in section 7.1. Nonetheless, we can observe some composition above the reference front, approaching the optimal state.

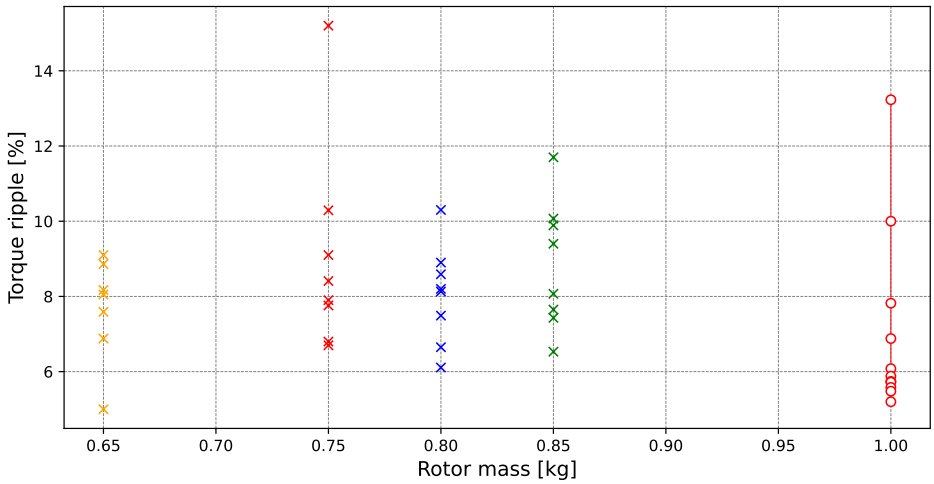

Figure 5.5: Rotor mass and torque ripple

From Figure 5.5 we can observe that no resultant topologies improve the cogging performance of the reference model. The lowest torque ripple obtained arise from a design where the rotor mass is equal to 0.65 [kg].

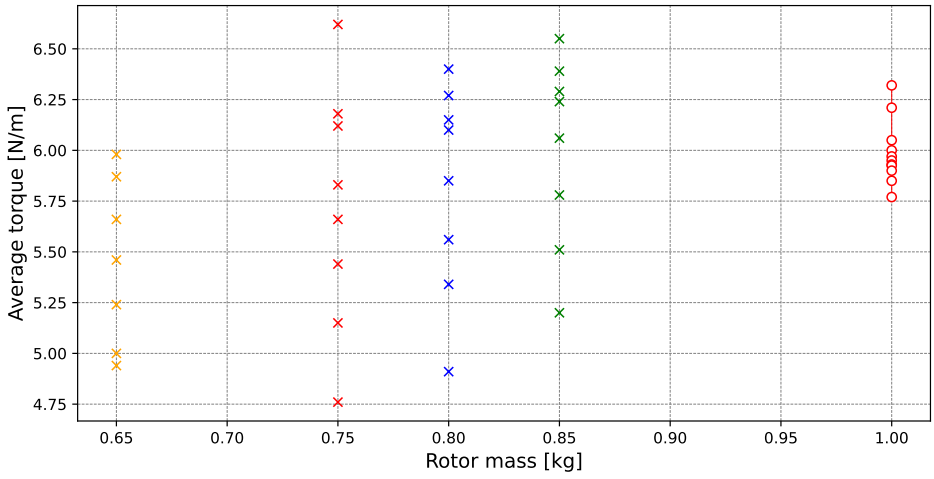

Figure 5.6: Rotor mass and average torque

Finally, from Figure 5.6 we can observe that some optimization results have better average torque performance while having lower masses compared to the reference model. This result indicate that the new rotor topology has the potential

to achieve a better torque-to-weight ratio compared to the reference model.

5.2.4 Design choice

Figure 5.7 provides a comparison between the reference Pareto front and the four topologies from each dataset that approach the most the optimal performance state. Making a trade-off between the multiple performance indices is crucial in determining the optimal design configuration.

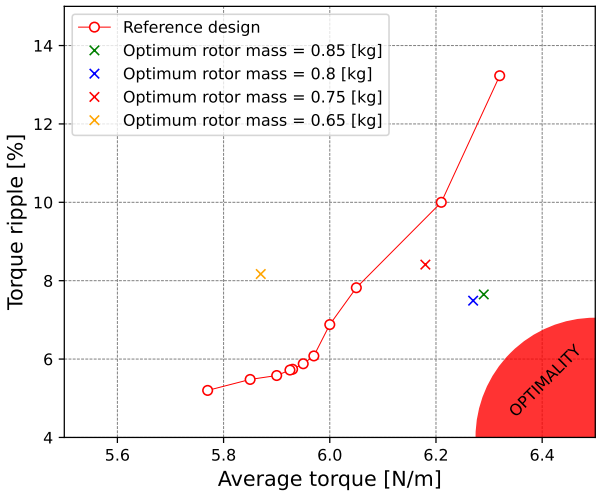

Figure 5.7: Optimal rotor topology from each data set

The most important objective will be to maximize the average torque. This is a crucial aspect for maximizing the power-to-weight ratio of the motor, which is highly desirable in order to enhance overall motor performance. The objective is to provide a configuration capable of producing higher or similar torque performance while reducing the rotor weight.

The second critical design aspect is the overall rotor mass. As stated at the outset of this thesis, one of the main objectives of topology optimization is to reduce motor mass in order to achieve weight savings in the design. Therefore, the design choices will involve finding a balance between minimizing mass and maximizing average torque

On the other hand, the torque ripple has not been explicitly considered during the topology optimization process. We have limited control over this parameter in our study. Moreover, the impact of the motor ripple on the vehicle performance is highly dependent on other parameters of the complete powertrain assembly. As a result, the weight given to torque ripple in our consideration is relatively low. However, it is important to note that the consideration of the torque ripple should not be completely omitted. In section 7.1, we will discuss the limitations of this research paper and provide suggestions for further developments to explore and

address the influence of torque ripple on motor performance.

From those considerations, the optimal topology is corresponding to the rotor mass of 0.75[kg]. This new reference model was chosen to pursue the design process. It offer a good trade-off between having a minimal weight and offering high torque performance.

5.3 Design post-processing

As explained in section 4.2, the outcome of the topology optimization process is typically further refined to accommodate manufacturing constraints and ensure practicality in real-life applications. This section focuses on the fine-tuning of the new reference topology to propose a final design that is better aligned with the manufacturing standards and implementation to the current in-wheel drivetrain.

5.3.1 Rotor core

The irregular shapes arising from the topology optimization are refined and simplified by more conventional forms of components. Figure 5.8 illustrates the evolution of the design during the post-processing stage.

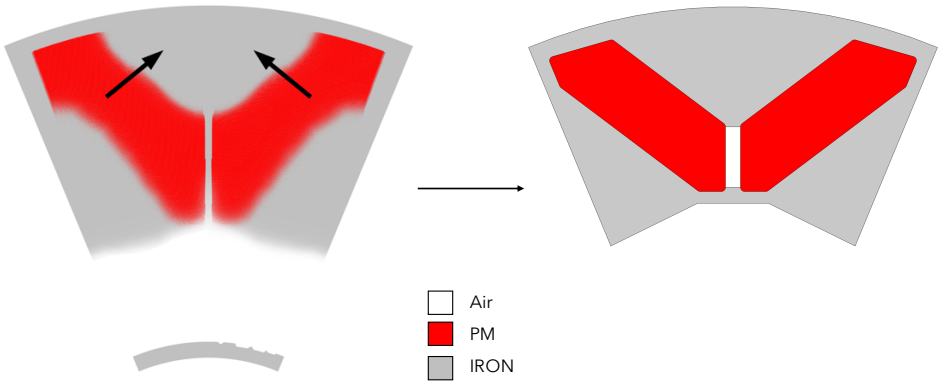

Figure 5.8: Reference topology (left) and post-processed rotor design (right)

First, we have removed the lower iron region of the design. As observed in 5.2.1, the lower iron area is not contributing to the torque generation allowing to save a significant amount of weight. Secondly, the magnets buried in the rotor are modelled with a rectangular shape instead of the initially complex geometry[4]. This change in shape makes the manufacturing process more conventional for permanent magnets.

In addition to the simplification of the iron and permanent magnets shapes, two notable design elements were added and optimized:

[4]The optimum height, width and position of the permanent magnets where found by using the same multi-objective parametric optimization procedure details in 5.2.3.

- A centered air pocket is placed between the two magnets. This added element helps to reduce the inductance along the rotor d-axis, leading to an increase of the reluctant torque contribution. By doing so, the average torque produced by the machine is increase without significantly modifying the cogging level. This means that the absolute cogging oscillation remains constant, while the relative cogging is decreased. Figure 5.9 shows the torque produce by the same rotor configuration, with the only exception of the presence of the central air bridge.

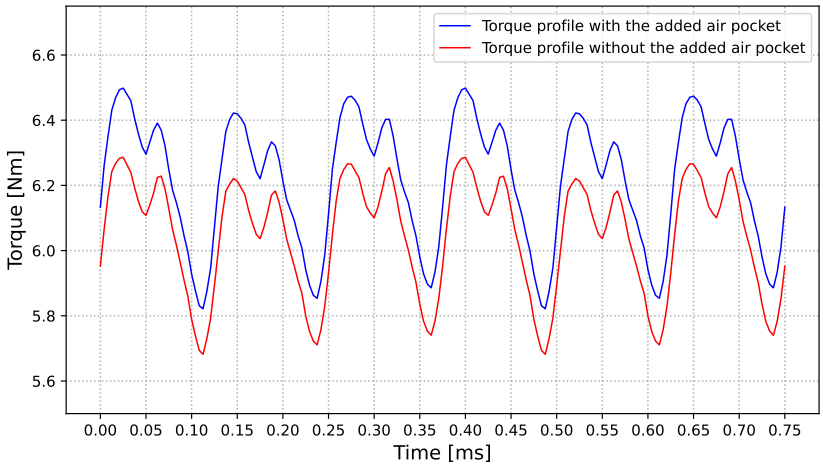

Figure 5.9: Effect of the added air pocket on the torque performance

For this particular example, the average torque is increased by 3% while the torque ripple is increased by less than 1%.

- Iron is strategically added under the air pocket bellow the two magnets. This placement enhances the structural integrity of the rotor, providing support and stability to the V-shape permanent magnets configuration. While this modification has a certain impact on the overall mass of the assembly (around 3%), it mainly reduces the stresses acting locally on the permanent magnets corners. We can observe in Figure 5.10[5] the structural benefit of the added iron to join the two half's of the rotor pole.

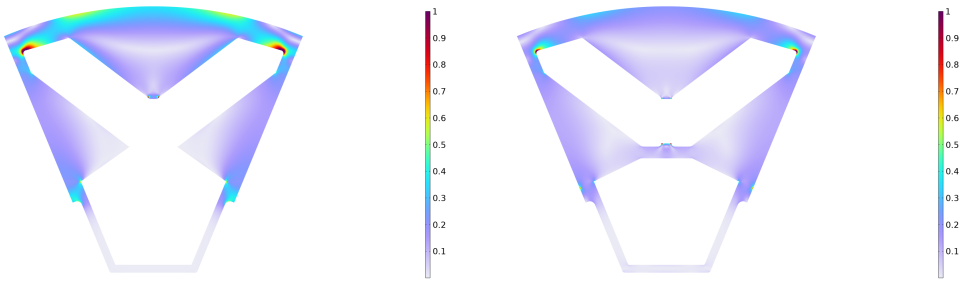

Figure 5.10: Effect of the added iron bridge: von Mises criterion

[5]The design of the added linkage structure visible on the lower part of the iron core will be covered in 5.3.2.

5.3.2 Shaft linkage

The resultant optimal rotor design has substantial differences in dimensions compared to the initial motor concept. One notable observation is that a significant portion of the iron core can be eliminated, resulting in weight savings. However, to ensure compatibility between the new rotor design and the current powertrain, two approaches can be considered:

1. Redesigning the powertrain: In this approach, the powertrain components, such as the shaft mainly and other supporting structures, are modified or redesigned to accommodate the new rotor. This may involve adjusting the dimensions, positions, or attachment points of these components to ensure proper alignment and functionality with the optimized rotor.

2. Adapting the Rotor Design: alternatively, the rotor design can be adapted to fit the existing powertrain components. This approach involves making adjustments to the optimized rotor configuration, such as adding support structures to assure the mechanical linkage with the rotating shaft.

For the purpose of this thesis, the focus will be on investigating the second approach. The objective is to find a balance between maintaining the weight savings achieved through the optimization and ensuring that the adapted rotor design can be seamlessly integrated into the existing powertrain system. By exploring this approach, the thesis aims to provide insights into the feasibility and challenges associated with adapting the rotor to meet the requirements of the current in-wheel setup. To design the support structure joining the new rotor and the existing shaft we need to considered several aspects.

First of all, in selecting the material for the new element structure, it is crucial to prioritize those that exhibit a favorable strength-to-density ratio. Given that the main objective of the linkage is to contribute to the overall robustness of the motor, the chosen materials should possess significant tensile strength while introducing minimal additional mass to the assembly. Furthermore, as the primary function of the linkage element is to transmit torque from the rotor to the shaft, twisting or torsional stresses are applied on the joining element. The design must be able to withstand the torque without failure.

In addition, it is important to ensure that the selected solution has a minimal impact on the magnetic circuit of the rotor. This requires selecting materials with low permeability to avoid disturbing the flux lines within the core. Low permeability materials have a reduced ability to conduct magnetic flux, which helps maintain the integrity of the magnetic circuit in the rotor. By minimizing the influence on the flux lines, the selected materials can preserve the efficiency and performance of the motor.

The following proposed materials align with the desired characteristics of both strength-to-density ratio and low permeability for the element:

- Carbon fiber reinforced polymers: this kind of composites offer excellent strength-to-density ratios and are widely used in the automotive industry. They have high tensile strength, low density, and can be tailored to have low permeability, making them suitable for maintaining the magnetic circuit integrity. In addition, the team has a lot of experience when manufacturing carbon fiber reinforced polymers, making it a favorable choice. In fact, such material is used to build the monocoque and the aerodynamic package. However, the dimensions involved and the complexity for the linkage element can induce additional challenges that could limit the manufacturability of the components.

- Titanium Alloys: titanium alloys exhibit excellent strength-to-density ratio and possess good tensile strength. This mainly explains why they are used in many Aerospace application. While titanium has slightly higher permeability than non-magnetic materials, specific titanium alloys can be selected to minimize their impact on the magnetic circuit. This material can be machined to fit perfectly the current powertrain configuration.

Obviously this is not an exhaustive list of all the compatible materials that can be used for such application. We can understand that the design of the supporting structure for the rotor could be a topic of dedicated study on its own, considering the complexity and importance of ensuring the structural integrity while minimizing the impact weight of the element.

However, for the purpose of this thesis, a simplified approach will be taken. What is commonly adopted in rotor design is to use soft-iron from the core to form the joining element. While the addition of iron can have an impact on the magnetic properties of the rotor, it is still a viable solution that simplifies the manufacturing process. By incorporating iron as a connecting element, the need for a separate attachment system or the use of additional materials with different properties can be avoided.

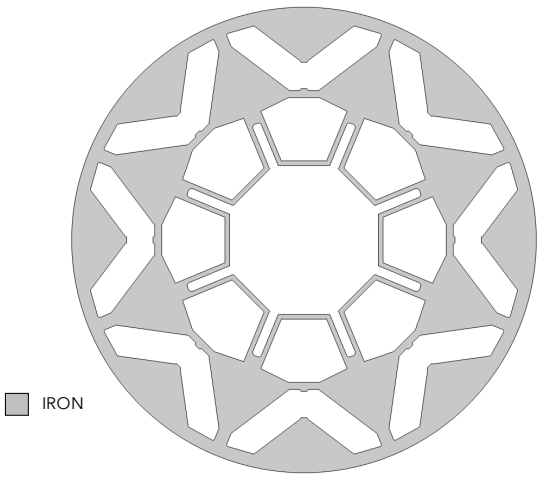

Figure 5.11: Finale rotor core and linkage system design

Figure 5.11 illustrates the complete rotor sector with the added iron structure that serves as a supporting element. The design of the iron extension is specifically tailored to accommodate the existing shaft employed by the team. The additional iron structure facilitates the connection between the rotor core and the shaft, ensuring a robust linkage. It also effectively restricts the tangential degree of freedom of the rotor when assembled onto the shaft. This is achieved through the incorporation of spikes or extensions on the shaft design, which prevent any relative rotation between the two elements. Consequently, this configuration enables the efficient transmission of torque from the rotor core to the shaft and ultimately, to the wheels. Figure 5.12 presents the geometry of the motor's shaft.

To explore the feasibility of using a different materials for the rotor supporting element, we modeled a titanium component concept as an alternative to the design choice linkage. When introducing a new component in the assembly, it becomes necessary to consider the mechanical link required to attach the rotor iron core to the rotor supporting element. In this context, the mechanical linkage refers to the structural connection between the rotor iron core and the titanium component. This linkage serves to securely fasten the core to the supporting element, ensuring stability and efficient transfer of forces during operation.

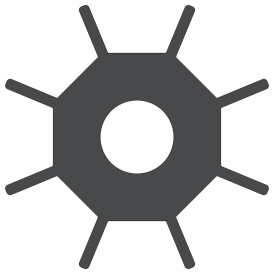

Figure 5.12: Motor's shaft

To do so, a devotail system is used. This kind of system is notably used to attache turbine blades to the shaft in a jet engines and other aerospace applications. In fact, this system is know for its very good tensile strength. Figure 5.13 presents the titanium linkage system concept and 5.14 illustrates the devotail joinery technique. This concept was tested under nominal loading conditions and assure the structural integrity of the assembly.

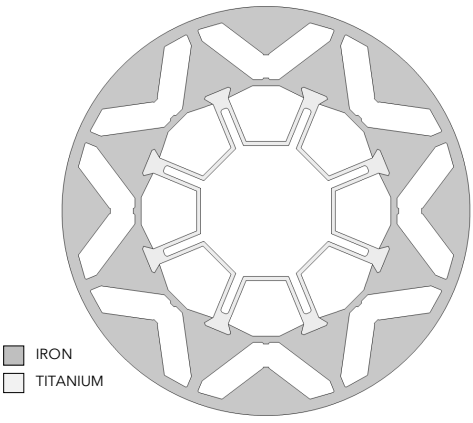

Figure 5.13: Titanium concept

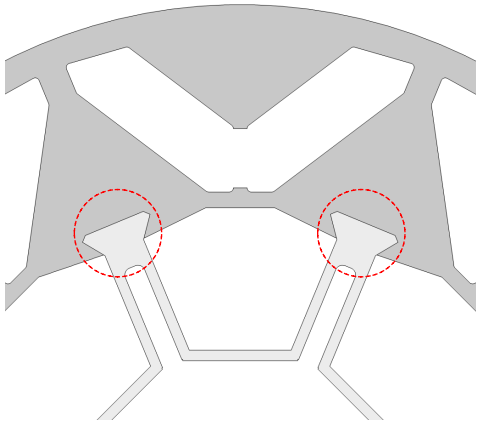

Figure 5.14: Devotail joinery system

The titanium system was able to yield a 3% reduction of the overall rotor mass assembly compared to the final design choice using conventional soft-iron. While this system proves that further mass reduction can be obtained, more meticulous design should be made to find the optimal titanium joining design and further test its impact on the magnetic circuit.

Nonetheless, the aim was to show the potential of such design but consequently also prove that the solution using iron still proposes very good weight saving while reducing the development effort required.

5.4 Final design

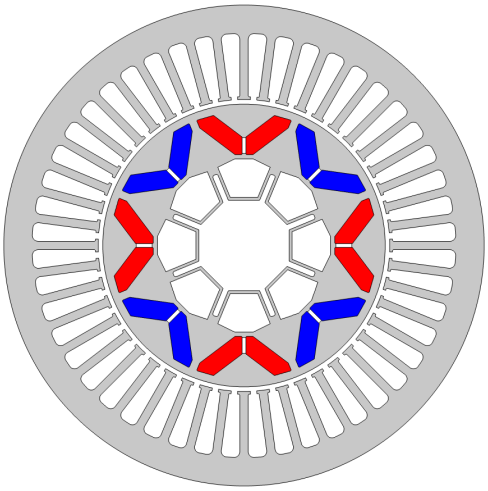

Figure 5.15: Complete motor assembly

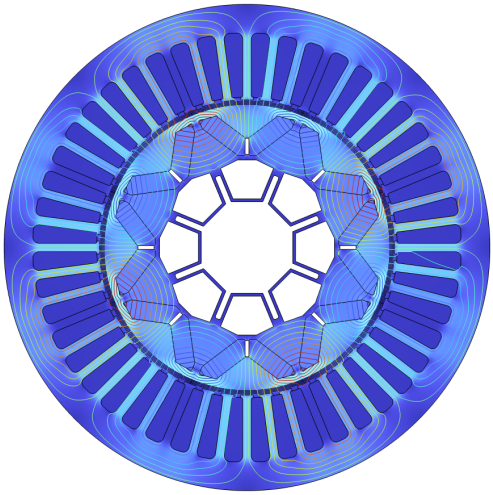

Figure 5.16: Magnetic flux and magnetic potential A_z solution

Figure 5.15 presents the completely new design of the motor topology. The new motor is composed of eigth magnetic poles. Each pole is made of two permanent magnets placed in a V-angle configuration. This new motor respects the geometry of the current powertrain used by the team, meaning its integration should not require any major modification of other components inside the in-wheel system. Figure 5.16 presents the solution of the magnetic flux and magnetic potential A_z, highlighting the eigth magnetic rotor poles and flux path.

5.5 Model comparison of optimal machines

We can finally compare the performance of the new motor with the reference spoke concept. The two motors where simulated with the same exact operating conditions[6]. Figure 5.17 illustrates the relationship between average torque and

[6]The tests was conducted at 20000[RPM] and with a current density of 5[A/mm^2]

torque ripple for the different motors considered.

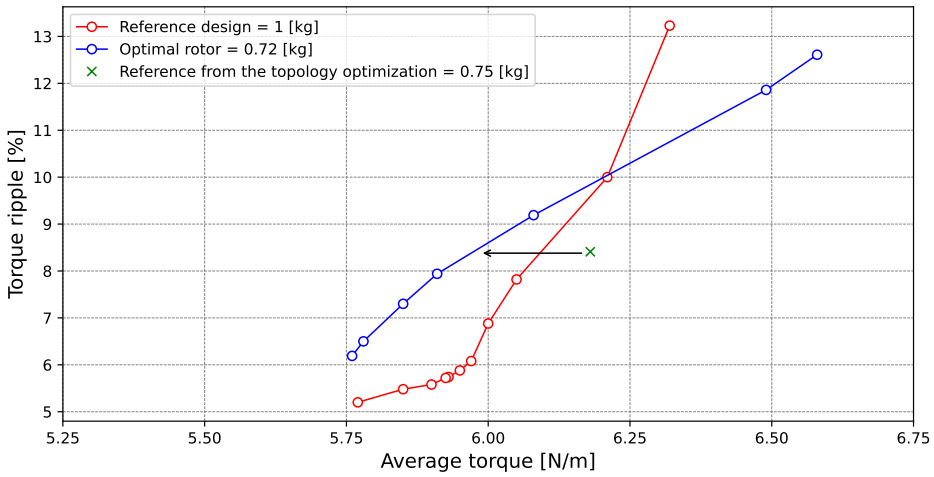

Figure 5.17: Optimal rotor topology from each data set

The first observation we can make concerns the post-processing of the topology optimization results. In the presented figure, the black arrow represents the post-processing design step discussed in subsection 5.3.1, which involves the approximation and interpretation of the topology optimization outcome. It is evident to see that this process resulted in a 19% decrease of the average torque for the closest final rotor design, measured at a constant torque ripple level. This observation highlights the limitations of the topology optimization and the importance of the post-processing step. It can be anticipated that the topology optimization produces idealistic outcomes, primarily unconstrained by manufacturing considerations. The approximation of the emerging shapes contributed to a decrease in torque performance. On the other hand, the refined final design was able to yield a 4% reduction of mass.

Secondly, the preceding figure compares the performance of the optimized and reference design. Each performance curve was obtained through the multi-objectives parametric optimization detailed in 5.2.3. We can see that the optimized model provides far better performance for high ripple values, but the tendency is reversed in the low ripple range.

For further analysis we will consider the two rotor design configuration which induce the lowest amount of cogging torque. Table 5.3 provides the details performance values of the these two motors:

	Optimized rotor	Reference rotor
Average torque	5.76 [Nm]	5.77 [Nm]
Torque ripple	6.19 [%]	5.2 [%]
Rotor weigth	0.72 [kg]	1 [kg]
Torque-to-weigth ratio	8	5.77

Table 5.3: Performance comparison

We can conclude that the new rotor is able to achieve a 28% weight reduction but comes with a decrease of average torque of 0.17% and an increase of torque ripple of 19%. While the decrease of average torque is clearly negligible, the increase of the torque ripple can be a limitation. Nonetheless, the overall torque-to-weigth ratio of the motor was increased by 38 %.

It is important to highlight that the new rotor design utilizes a significantly lower quantity of magnets compared to the reference model. The optimized design incorporates magnets with a surface area of 56.4 [mm^2], whereas the spoke topology utilizes magnets with a surface area of 81.6 [mm^2]. This results in a substantial reduction of 30% in the total magnet mass used. The optimization process demonstrates the potential to enhance the utilization of magnetic material within the rotor structure.

6 | Optimal design performance and analysis

This chapter will provide an comprehensive analysis of the new rotor performance. We will first focus on the electromagnetic torque characteristics and follow by a structural analysis.

6.1 Torque Characteristics

This section propose a in depth analysis of the torque performance of the optimized rotor. We will first analyse in total torque ripple and then separate the total torque into its magnetic and reluctant contributions. We will follow by an evaluate of the harmonic content of the resultant signals.

6.1.1 Torque ripple and contributions

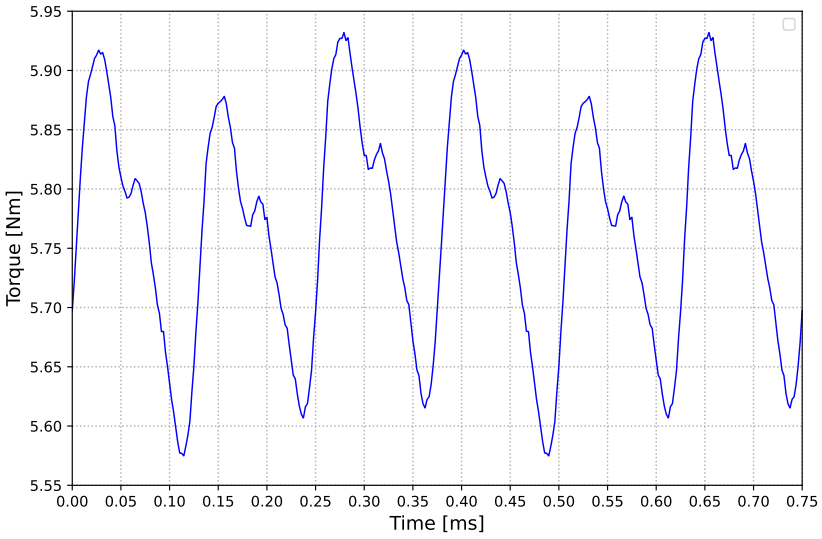

Figure 6.1: Torque ripple waveform

Figure 6.1 presents the torque waveform evaluated over one electrical period at 20000 [RPM] with a current density of 5 [A/mm^2]. Table 6.1 presents the quantitative performance of the new rotor.

Performance indices	Values
Average torque	5.76 [Nm]
Torque ripple	6.19 [%]

Table 6.1: Optimized rotor performance at specific operating point

As discussed in the previous chapters, the torque of a IPM motor results from a combination of magnetic and reluctance torque contributions. Separating the total torque into its magnetic and reluctance components provides a deeper understanding of the underlying physical mechanisms at work in an our new motor. Each torque component can be isolated and measured with a judicious current distribution along the rotor d- and q- axis.

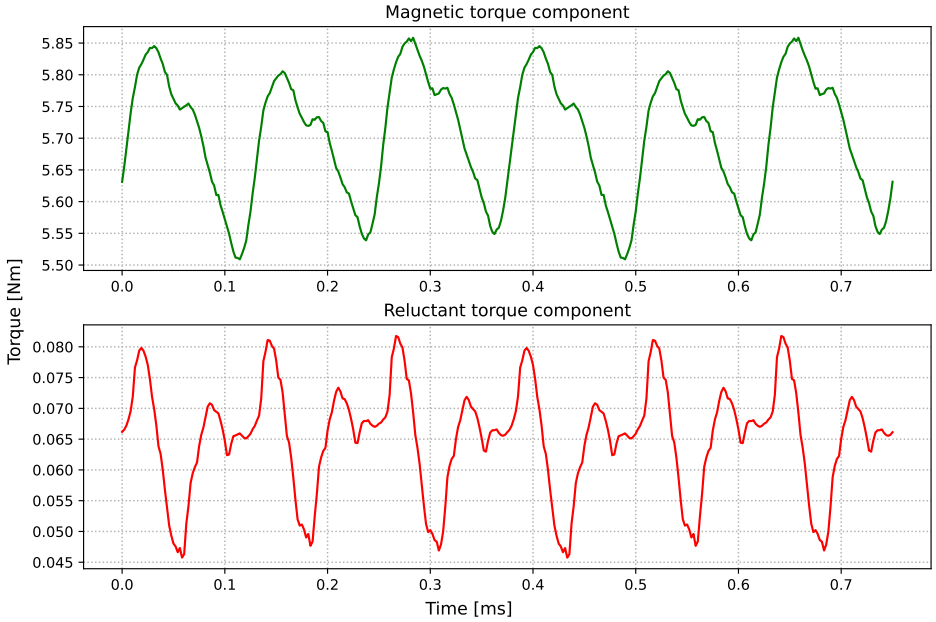

Figure 6.2: Magnetic and reluctant torque components waveforms

Figure 6.2 shows the separated torque components. The magnetic torque was obtained by injecting current only along the rotor q-axis, i.e. by imposing a electrical phase angle of 0 [°]. On the other hand, the reluctant torque was obtained simply by subtracting the magnetic component to the total torque. Table 6.2 details the numerical values of the different contributions. We can see that the majority of the torque is produced by the magnetic contribution.

	Magnetic component	Reluctant component
Average value	5.703 [Nm]	0.065 [Nm]
Contribution to total torque	98.88 [%]	1.12 [%]

Table 6.2: Torque contributions: numerical values

Finally, Figure 6.3 illustrates the optimal electrical angle required to achieve maximum torque performance. The optimal state is determined to be -8 [°]. This implies that the stator voltage phasor is positioned beyond the rotor q-axis. This phenomenon arises from the fact that the inductance along the q-axis exceeds the inductance along the d-axis. Indeed, the presence of an additional central air pocket contributes to a higher reluctance along the d-axis compared to the q-axis. Consequently, the inductance along the d-axis is lower. Referring to torque equation 4.6, it becomes evident that with the aforementioned scenario, the contribution of the reluctant torque is negative since the term $(L_d - L_q)$ is negative. As the electrical phase angle is situated below 0 [°], the current i_d becomes negative, resulting in a change of sign for the reluctant component $(L_d - L_q)$, and finally a positive contribution to the overall torque.

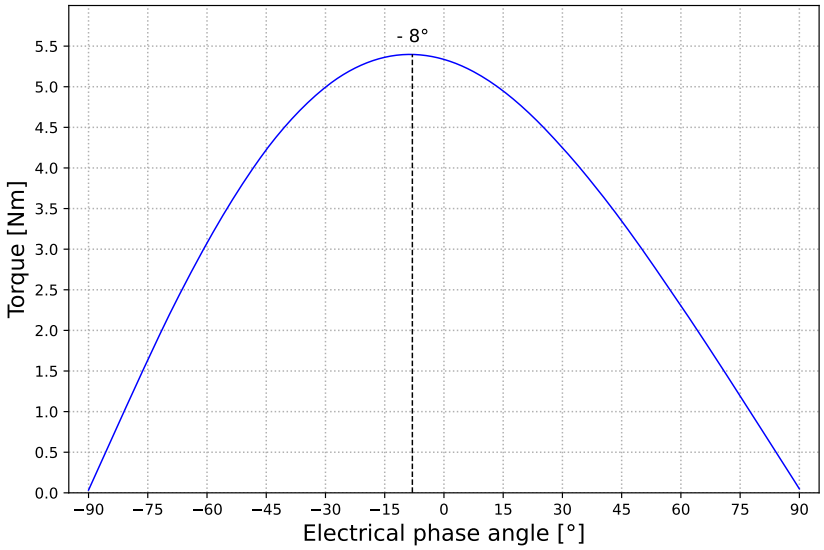

Figure 6.3: Optimal electrical phase angle

6.1.2 Torque harmonic content

As we have see previously, the cogging torque of the new rotor is increased compared to the reference model. While this can be a limitation of the design, it is important to study the frequency content of the oscillating signal.

In fact, by analyzing the frequency content of the cogging torque, it becomes possible to identify specific frequency components that contribute to noise and vibration issues. This knowledge can then be used to develop appropriate mitigation strategies to reduce or eliminate these adverse effects. It indeed allows for the identification of potential areas of improvement, such as the reduction of specific harmonics or addressing resonance-related issues to enhance the overall performance and stability of the motor.

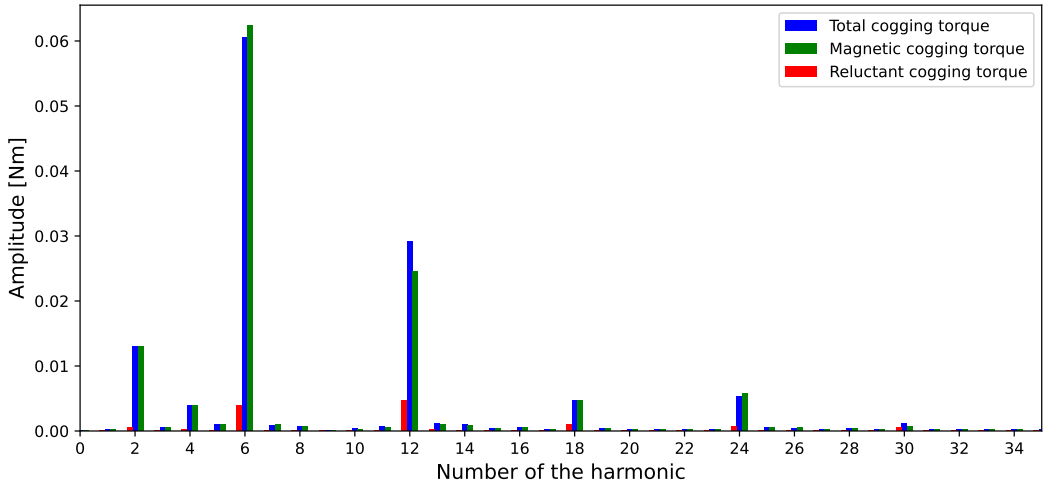

Figure 6.4: Harmonic content of the torque waveforms

Figure 6.4 presents the harmonic content of the cogging torque characteristics measured over one electrical period at 20000[RPM]. In this figure, the total torque is present along its magnetic and reluctant component. To obtained those results, we simply subtracted the DC-component (the average values) to the different waveforms and performed a discrete fourier transformation.

The analysis of the cogging torque reveals that the dominant harmonic is the 6th harmonic. This harmonic contributes to approximately 16% of the total cogging oscillation, with a magnitude not exceeding 0.06 [Nm]. Similarly, in the case of the magnetic cogging contribution, the dominant harmonic is also the 6th harmonic, contributing to around 17.7% of the magnetic cogging oscillation, with a magnitude not exceeding 0.062 [Nm]. Additionally, the dominant harmonic of the reluctant contribution is the 12th harmonic, contributing to approximately 15.78% of the magnetic cogging oscillation, with a magnitude not exceeding 0.006 [Nm].

It is worth noting that the presence of dominant harmonics at the 6th, 12th, 18th, and 24th harmonics indicates the potential existence of resonant modes within the system. Resonance can occur when the excitation frequency aligns with the natural frequency of the system, leading to increased vibrations and potential stability concerns.

6.2 Mechanical aspects

This section presents the structural analysis of the new rotor topology. The mechanical behavior of the rotor was tested at the maximum operating conditions of 20000 [RPM]. This critical speed was chosen based on the current utilisation of the motor by the Formula team. For speed above this threshold, the structural integrity of the rotor may not be assured.

6.2.1 Rotor loading

As stated in subsection 4.4.2, the rotor is subject to both volume and surface forces.

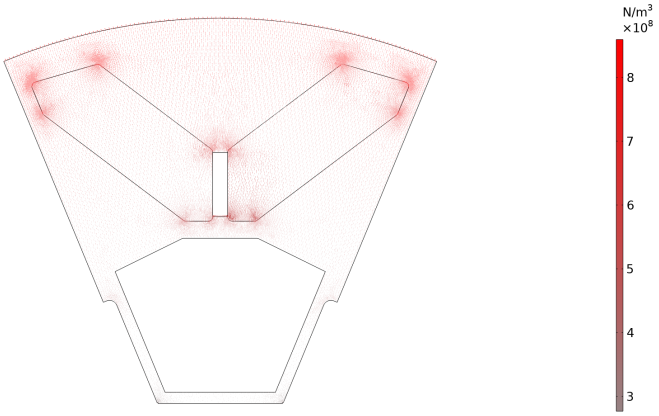

Figure 6.5: Volume forces distribution

Figure 6.5 illustrates the volume forces applied to the system resulting from the centrifugal effect. This centrifugal load is primarily concentrated near the corners of slots dedicated to the buried permanent magnets in the rotor. These corners tend to act as stress concentrators, where stress and strain tend to accumulate. The corners experience higher stress concentrations compared to the straight sections of the slot because they create geometric irregularities that disrupt the uniform distribution of stress within the material, leading to localized stress concentrations.

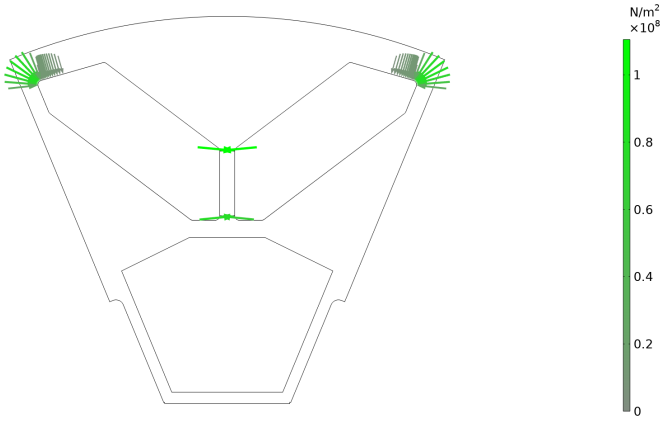

Figure 6.6: Contact forces distribution on the permanent magnets

Figure 6.6 illustrates the resultant contact forces acting on the permanent magnets as they are retained by the iron core. The visualization reveals that the load is primarily concentrated on the upper corners of the permanent magnets, indicating a potential vulnerability to mechanical failure in this region. Some contact reaction can also be expected on the small iron extensions situated between the two magnets.

6.2.2 Stresses and displacement

Figure 6.7 presents the von Mises analysis of the new rotor structure. As recall from subsection 4.4.1 the von Mises criterion is expressed as:

$$\sigma = \frac{\sigma_v}{\frac{S_y}{SF}} \tag{6.1}$$

where σ is the depicted normalized von Mises stress, σ_v is the actual von Mises stress, S_y is the iron yielding strength and SF the safety factor.

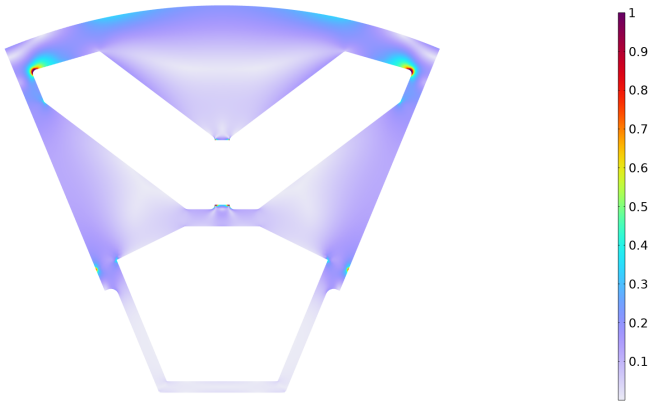

Figure 6.7: von Mises criterion: stress distribution

In line with the previous results, the analysis show that the critical regions under maximum loading conditions are situated on the upper corners of the slots dedicated to the permanent magnets. It is important to note that the rotation speed of 20000 [RPM] is not a nominal working condition for the motor, and this state of operation is usually sustained for only a few milliseconds. As a result, minor regions that exceed the von Mises threshold can be tolerated within this short duration.

However, it is important to ensure that the magnitudes and duration of these stress concentrations are carefully evaluated and compared against the material's fatigue strength and other relevant design considerations. This will help guarantee that the motor can withstand the occasional high-stress events without compromising its long-term reliability and durability. Further analysis and validation, including fatigue life assessments, can provide a more comprehensive understanding of the structural behavior and potential failure risks under extreme loading conditions.

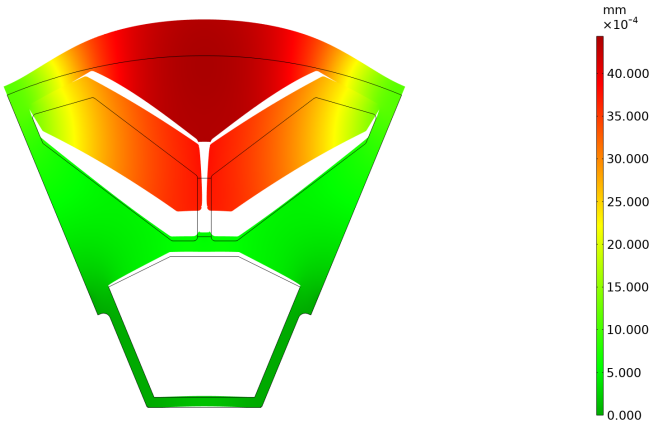

Figure 6.8: Rotor displacement

Finally, Figure 6.8 shows the displacement motion of the rotor sector due to the loading condition. For better visualization, the displacement has been scaled by a factor of 250. The maximum displacement observed at 20000 [RPM] is 0.005 [mm]. This displacement value is well within acceptable limit range, indicating that the rotor structure maintains its geometry even at high speeds. The observed displacement values indicate that the rotor design is robust and can withstand the centrifugal forces and mechanical stresses encountered during high speed operation.

7 | Discussion

This chapter will express the limitations encountered during the research and present some improvements and suggestions for pursuing the development of the complete motor.

7.1 Limitations of modelling and optimization

As discussed all along this research study, some limitations must be highlighted for future work and reference.

1. Data limitations: the optimization is compared based on the performance of a reference motor design. However, as stated at the beginning of this paper, very little information is available regarding the current motor geometry. The lack of detailed knowledge about the motor's configuration poses a challenge in accurately modeling it. While we developed a method to replicate the operation of the real motor concept as closely as possible, achieving a 100% accuracy in replicating the system behavior without additional informations on its geometry is not feasible.

2. Topology optimization step: as discussed in 5.1.1 the objective function of the topology optimization study focuses solely on maximizing the average torque performance. While the average torque is a crucial characteristic, the consideration of torque ripple would enhance the optimization process. This limitation arises from the implementation of the topology optimization in *Comsol Multiphysics®*.

   The gradient-based solver employed in this study, which utilizes the MMA, is designed to work with stationary study configurations. This explained why the average torque was obtained by discretizing the movement of the rotor and evaluating the torque for each of these configurations. In addition, the objective function can only be evaluated at the last stationary study step, prior to the solver iterating on the densities. This limitation prevents the inclusion of the torque ripple in the primary optimization process as we cannot access data to find the maximum and minimum torque values. Consequently, the optimized rotor design exhibit slightly higher torque ripple values compared to the reference design

7.2 Further improvements and suggestions

While the proposed rotor concept has demonstrated promising performance results, there are still opportunities for improvement for future work on this project.

First and foremost, addressing the limitation of the new rotor concept in terms of cogging performance is of utmost importance for further investigations. Cogging torque is a complex phenomenon influenced by various factors, making its reduction a challenging task. However, there are several ideas that can be pursued to minimize the cogging content:

1. As we have briefly explained in 3.1.1, the winding factor of a motor, denoted as k_w, plays a crucial role in achieving high winding performance. The winding factor can be expressed as follows:

$$k_w = k_p \cdot k_d \cdot k_s \tag{7.1}$$

   where k_p is the pitch factor, k_d is the distribution factor, and k_s is the skewing factor of the motor. While it is beyond the scope of this study to delve into the details of each contribution to the winding factor, optimizing these subfactors can lead to improved torque ripple performance. This optimization process may involve examining the complete stator assembly, exploring different options for the number of poles, and considering other design parameters that can influence the winding factor. By carefully analyzing and optimizing these individual factors, it is possible to enhance the winding performance of the motor and reduce the cogging content.

2. An additional optimization that focuses on minimizing the cogging torque of the rotor design can offer significant benefits. Various techniques can be employed to reduce this component without modifying other composing parts. One effective approach is the incorporation of air pockets within the rotor structure. These features consist of simple air gaps placed strategically, typically at the corners of the permanent magnets. Their purpose is to minimize the short-circuit magnetic path generated by the magnets. Figure 7.1 presents an example of such structures.

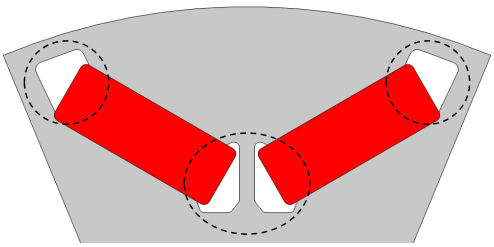

Figure 7.1: Example of air pockets around permanent magnets

   By introducing air gaps into the design, the permeability along the flux path is reduced, preventing the recirculation of the flux. The use of air bridges

and air ribs can effectively lead to a reduction in cogging torque. In addition, the optimization of the air bridges can be implemented without significant modifications to other motor components, making it a interesting solution for improving the overall performance of the motor.

Another crucial element that can contribute to significant improvements in reducing the motor's weight and enhancing the power-to-weight ratio is a judicious selection of materials. During this study, generic metals commonly used in electric motors and readily available in the market were employed. However, the exploration of more advanced and complex materials holds the potential to further enhance motor performance while reducing weight.

The choice of materials have a profound impact on various aspects of motor design, including magnetic properties, mechanical strength, thermal conductivity, and overall efficiency. By leveraging advanced materials such as high-performance alloys, composite materials, or even lightweight and durable polymers, it is possible to achieve higher power densities and improved motor efficiency. Furthermore, the use of advanced materials consisting the core of the motor can offer advantages in terms of reducing eddy current losses, minimizing hysteresis losses, and enhancing thermal management.

8 | Conclusion

8.1 Results summary

The study introduced a novel rotor concept specifically designed for high-speed applications. This new rotor configuration demonstrated comparable torque generation to the reference motor concept while operating under the same conditions. However, the significant advantage of the new rotor concept was its remarkable weight reduction of 28%, leading to a substantial increase in the power-to-weight ratio of the motor assembly by 38%. Additionally, the optimization of materials distribution led to a 30% reduction in the quantity of permanent magnets used.

Although the weight reduction and improved power-to-weight ratio were notable achievements, it is important to acknowledge that the new rotor design exhibited a 19% increase in torque ripple. This indicates a certain level of instability in the torque output, suggesting the need for further improvements in this aspect.

A visual representation of the new rotor configuration can be observed in Figure 8.1.

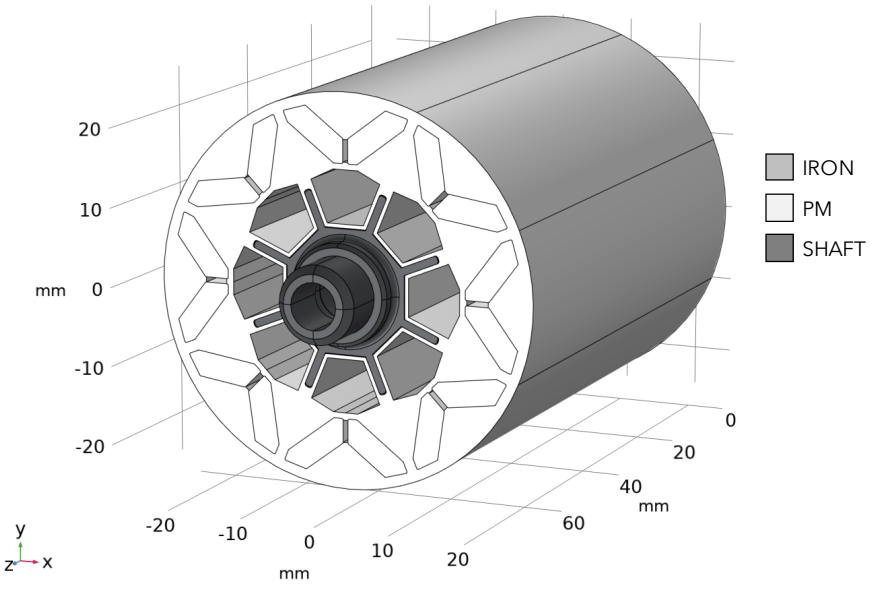

Figure 8.1: 3D model of the optimized rotor mounted on its shaft

8.2 Final note

Despite some limitations encountered during this study, the achieved results can be considered highly promising and significant in terms of meeting the primary objectives of the project. The main focus was to reduce the weight of the rotor while maintaining high motor performance, ultimately increasing the overall power-to-weight ratio of the assembly.

The obtained results demonstrate that the new rotor concept successfully achieved these objectives. By implementing the optimized rotor design, a notable reduction in rotor weight was achieved without compromising the motor's performance capabilities. This resulted in a substantial improvement in the power-to-weight ratio, which is a crucial factor in high-performance applications such as those encountered in *Formula Electric Belgium*.

Moreover, this study has also showcased the effective utilization of topology optimization techniques specifically tailored for electric motor applications. By employing these advanced optimization methods, we were was able to generate an initial iteration of an optimal rotor concept, providing valuable insights and a solid foundation for further development and refinements.

The outcomes of this research not only demonstrate the potential of the new rotor concept but also lay the groundwork for future iterations and improvements in the design. With more detailed information on the motor's geometry and the inclusion of optimization techniques that consider torque ripple, it is expected that the performance of the rotor design can be further enhanced.

In conclusion, the results of this study have proven to be highly promising, successfully achieving the project's primary objectives. The optimized rotor concept, along with the demonstrated utilization of topology optimization techniques, paves the way for future advancements in the motor design and contributes to the ongoing progress in the field of high-performance electric motors.

References

[1] P. A. Aune, "a Four Wheel Drive System for a Formula Style Electric Racecar," Master thesis, NTNU, 2016. Accessed: May 05, 2023. [Online]. Available: https://ntnuopen.ntnu.no/ntnu-xmlui/handle/11250/2384523 [Accessed: March. 5, 2023]

[2] "Emetor - Glossary - Winding factor." [Online]. Available:https://www.emetor.com/glossary/winding-factor/ [Accessed May 10, 2023].

[3] M.-H. Hwang, J.-H. Han, D.-H. Kim, and H.-R. Cha, "Design and Analysis of Rotor Shapes for IPM Motors in EV Power Traction Platforms," Energies, vol. 11, no. 10, p. 2601, Sep. 2018. [Online]. Available: https://www.mdpi.com/1996-1073/11/10/2601 [Accessed May 10, 2023].

[4] "Diabatix - Topology optimization vs Generative design." [Online]. Available: https://www.diabatix.com/blog/generative-design-topology-optimization-and-parametric-optimization-what-are-the-differences [Accessed May 13, 2023].

[5] O. Sigmund and K. Maute, "Topology optimization approaches," Struct Multidisc Optim, vol. 48, no. 6, pp. 1031–1055, Dec. 2013. [Accessed May 17, 2023].

[6] H. A. Eschenauer and N. Olhoff, "Topology optimization of continuum structures: A review*," Applied Mechanics Reviews, vol. 54, no. 4, pp. 331–390, Jul. 2001. [Accessed May 21, 2023].

[7] M. P. Bendsøe and N. Kikuchi, "Generating optimal topologies in structural design using a homogenization method," Computer Methods in Applied Mechanics and Engineering, vol. 71, no. 2, pp. 197–224, Nov. 1988. [Online]. Available: https://deepblue.lib.umich.edu/bitstream/handle/2027.42/27079/0000070.pdf;sequence=1 [Accessed May 06, 2023].

[8] "Energies | Free Full-Text | Optimal Design of Asymmetric Rotor Pole for Interior Permanent Magnet Synchronous Motor Using Topology Optimization." [Online]. Available: https://www.mdpi.com/1996-1073/15/21/8254 [Accessed May 06, 2023].

[9] [O. Korman, M. Di Nardo, M. Degano, and C. Gerada, "On the Use of Topology Optimization for Synchronous Reluctance Machines Design,"

Energies, vol. 15, no. 10, Art. no. 10, Jan. 2022. [Online]. Available: https://www.mdpi.com/1996-1073/15/10/3719 [Accessed May 06, 2023].

[10] K. Svanberg, "The method of moving asymptotes—a new method for structural optimization," Int. J. Numer. Meth. Engng., vol. 24, no. 2, pp. 359–373, Feb. 1987. [Online]. Available: http://paulino.princeton.edu/courses/cee307/2016/resources/papers/IJNME_MMA1987.pdf [Accessed May 15, 2023].

[11] "Topology Optimization for the Manufacturable and Structurally Safe Synchronous Reluctance Motors With Multiple Iron Webs and Bridges | IEEE Journals Magazine | IEEE Xplore." [Online]. Available: https://ieeexplore.ieee.org/document/9709207 [Accessed May 15, 2023].

[12] T.-H. Lee, J.-H. Lee, K.-P. Yi, and D.-K. Lim, "Optimal Design of a Synchronous Reluctance Motor Using a Genetic Topology Algorithm," Processes, vol. 9, no. 10, Art. no. 10, Oct. 2021. [Online]. Available: https://www.mdpi.com/2227-9717/9/10/1778/htm [Accessed May 15, 2023].

[13] "Multimaterial Topology Optimization of Electric Machines Based on Normalized Gaussian Network | Semantic Scholar." [Online]. Available: https://www.semanticscholar.org/paper/Multimaterial-Topology-Optimization-of-Electric-on-Sato-Watanabe/d2c73269215c674a9664b30628d9888b96e24830[Accessed May 27, 2023].

[14] "Gaussian network model," Wikipedia. Nov. 22, 2022. Accessed: Jun. 03, 2023. [Online]. Available: https://en.wikipedia.org/w/index.php?title=Gaussian_network_model&oldid=1123185929[Accessed May 01, 2023].

[15] "Evolutionary algorithm," Wikipedia. May 22, 2023. Accessed: Jun. 03, 2023. [Online]. Available: https://en.wikipedia.org/w/index.php?title=Evolutionary_algorithm&oldid=1156319244 [Accessed May 03, 2023].

[16] "Genetic algorithm," Wikipedia. May 25, 2023. Accessed: Jun. 03, 2023. [Online]. Available: https://en.wikipedia.org/w/index.php?title=Genetic_algorithm&oldid=1157003667 [Accessed May 07, 2023].

[17] H. Wu, S. Niu, and W. Fu, "Optimal Design of Asymmetric Rotor Pole for Interior Permanent Magnet Synchronous Motor Using Topology Optimization," Energies, vol. 15, no. 21, Art. no. 21, Jan. 2022. [Online]. Available: https://www.mdpi.com/1996-1073/15/21/8254 [Accessed May 07, 2023].

[18] "Adopting the Topology Optimization in the Design of High-Speed Synchronous Reluctance Motors for Electric Vehicles | IEEE Journals & Magazine | IEEE Xplore." [Online]. Available: https://ieeexplore.ieee.org/document/9134937 [Accessed May 07, 2023].

[19] "Keynote: Topology Optimization for an Efficient Design of an Electric Motor,"Comsol. [Online]. Available: https://www.comsol.com/video/key

note-topology-optimization-for-an-efficient-design-of-an-electric-motor [Accessed May 07, 2023].

[20] A. Harish, "What Is FEM & FEA Explained | Finite Element Method," SimScale, Oct. 24, 2016. [Online]. Available: https://www.simscale.com/blog/what-is-finite-element-method/ [Accessed May 05, 2023].

[21] N. Sadowski, Y. Lefevre, M. Lajoie-Mazenc, and J. Cros, "Finite element torque calculation in electrical machines while considering the movement," IEEE Trans. Magn., vol. 28, no. 2, pp. 1410–1413, Mar. 1992. [Online]. Available: https://hal.science/hal-01630020/document [Accessed May 12, 2023].

[22] J. S. Hsu, B. P. Scoggins, M. B. Scudiere, L. D. Marlino, D. J. Adams, and P. Pillay, "Nature and measurements of torque ripple of permanent-magnet adjustable-speed motors," Applied power and electronics conference and exposition, Dallas, TX (United States), 5-9 Mar 1995, Aug. 01, 1995. [Online]. Available: https://digital.library.unt.edu/ark:/67531/metadc619427/m1/1/ [Accessed May 07, 2023].

[23] "Emetor - Glossary - Torque ripple." [Online]. Available: https://www.emetor.com/glossary/torque-ripple/ [Accessed May 16, 2023].

[24] "What is Von Mises Stress in FEA? | SimWiki," SimScale. [Online]. Available: https://www.simscale.com/docs/simwiki/fea-finite-element-analysis/what-is-von-mises-stress/ [Accessed May 07, 2023].

[25] "Performing Topology Optimization with the Density Method," COMSOL. [Online]. Available: https://www.comsol.com/blogs/performing-topology-optimization-with-the-density-method/ [Accessed May 07, 2023].

Chat GPT, an AI-powered conversational agent developed by Open-AI was utilized as a collaborative tool during this thesis. It provided valuable assistance in generating structured ideas and proper paragraphs formulation, contributing to the clarity of this paper.

Zotero is a powerful reference management software that offers a range of features to assist researchers in organizing and citing their sources. This software was responsible for the proper formulation of the references in this thesis.

UNIVERSITÉ CATHOLIQUE DE LOUVAIN
École polytechnique de Louvain
Rue Archimède, 1 bte L6.11.01, 1348 Louvain-la-Neuve, Belgique | **www.uclouvain.be/epl**